High-K isomers and rotational structures in ^{174}W

S. K. Tandel, P. Chowdhury, and E. H. Seabury*
Department of Physics, University of Massachusetts Lowell, Lowell, Massachusetts 01854, USA

I. Ahmad, M. P. Carpenter, S. M. Fischer, R. V. F. Janssens, T. L. Khoo, T. Lauritsen, C. J. Lister, and D. Seweryniak
Physics Division, Argonne National Laboratory, Argonne, Illinois 60439, USA

Y. R. Shimizu
Department of Physics, Kyushu University, Fukuoka 812-8581, Japan
(Received 29 December 2005; published 11 April 2006)

High-spin states in ^{174}W ($Z = 74$) have been populated using the reaction ^{128}Te(^{50}Ti, $4n$)^{174}W at beam energies of 215 and 225 MeV. The Gammasphere array was used to detect the γ rays emitted by the evaporation residues. Four previously known collective band structures have been extended, and 16 new rotational sequences observed. Two are built upon isomeric states, one corresponding to a two-quasiparticle $K = 8$ isomer, the other to a four-quasiparticle $K = 12$ isomer, with the latter exhibiting strong K-violating $\Delta K = 12$ decays to the ground state band. Nucleonic configurations for the two- and four-quasiparticle excitations are proposed, and Woods-Saxon cranking calculations are presented to understand the rotational structures. Decay mechanisms of multi-quasiparticle K isomers are discussed in terms of the prevalent phenomenological models, with special emphasis on γ-tunneling calculations. Surprisingly, the latter underpredict the decay hindrance for the $K = 12$ isomer by three orders of magnitude, unlike all other isomer decays in this mass region.

DOI: 10.1103/PhysRevC.73.044306 PACS number(s): 23.20.Lv, 21.10.Tg, 21.60.Ev, 27.70.+q

I. INTRODUCTION

Nuclei with mass $A \approx 180$ provide excellent examples of the competition between few-particle excitations and collective rotation. The clarity of this interplay in this region stems primarily from the contribution of the quantum number K, the projection of the noncollective part of the total angular momentum on the symmetry axis of deformed nuclei. In $A \approx 180$ nuclei, both neutron and proton orbitals with large projections of the individual nucleonic angular momenta lie near the Fermi surface. This creates a favorable condition for the formation of high-K states, which can compete with collective rotation of the axially symmetric, well-deformed ground state as a means of generating angular momentum. The physics of the K quantum number, in itself, has remained a topic of interest in nuclear structure studies. K is an approximately conserved quantum number, and the decay of high-K states is, therefore, governed by selection rules. When the only available transitions involve a large change, ΔK, in K value, the decay is often hindered, leading to the phenomenon of K isomerism. A measure of the degree of forbiddenness of such decays is given by $\nu = \Delta K - \lambda$, where λ is the multipolarity of the transition involved in the decay. Following the advent of modern multidetector arrays, a number of K isomers have been observed with anomalously fast decay rates compared with previous expectations [1], and a considerable amount of experimental and theoretical effort has been focused toward understanding this phenomenon.

One of the primary motivations for this work was to investigate a specific novel mechanism invoked to explain these anomalous decays when conventional Coriolis mixing arguments seemed inadequate, namely, that of γ tunneling [2], where γ is the triaxiality parameter. In this scenario, large-scale, nonaxial fluctuations of the nuclear shape are thought to be responsible for the tunneling of the nucleus from a configuration with $\gamma = -120^\circ$ (prolate noncollective) to $\gamma = 0^\circ$ (prolate collective) through intermediate values of γ. Calculations based on this mechanism [2] have shown reasonable agreement with experimental data—as, for example, for the $K^\pi = 25^+$ isomer in ^{182}Os [3] and the $K^\pi = 14^+$ isomer in ^{176}W [4,5]—and have subsequently been shown to be able to reproduce a large number of such anomalous decays in this region [6].

The nucleus $^{174}_{74}$W, as a neighboring even-even isotope of ^{176}W, is an obvious candidate for a systematic test of this mechanism, especially given the previous observation of an isomeric state in this nucleus at modest spin, with a reported half-life of 187 ns [7]. For isomers in this half-life range, a γ-spectroscopy experiment with a wide time coincidence window of a few hundred ns can simultaneously map "prompt" band structures built on two-quasiparticle (2-qp) excitations, which help in assigning configurations to any observed multi-qp isomers. The present work describes the multiple new band structures observed in ^{174}W and the nucleonic configurations assigned to these bands. The feeding and decay of a new 4-qp, $K = 12$ isomer is discussed in specific detail, and a comparison of the observed hindrance factors with γ-tunneling calculations is provided. Preliminary results of this work have been presented earlier [8,9].

II. EXPERIMENT

High-spin states in ^{174}W were populated using the reaction ^{128}Te(^{50}Ti, $4n$)^{174}W at beam energies of 215 and 225 MeV.

*Present address: Idaho National Laboratory, Idaho Falls, Idaho 83415-3840.

The data obtained at both beam energies were summed during the analysis. The beam was provided by the 88-inch cyclotron at Lawrence Berkeley National Laboratory and was pulsed with a 70 ns period. The target consisted of a 1 mg/cm^2 ^{128}Te layer backed by 50 mg/cm^2 of ^{nat}Pb, thick enough to stop the evaporation residues. The γ rays emitted by the reaction products were detected using the Gammasphere array [10], with 91 Compton-suppressed germanium detectors. A total of 1.2×10^9 events that satisfied a prompt coincidence condition of the firing of four or more suppressed detectors were recorded to magnetic tape. In addition to the γ energies, the γ times with respect to the rf pulsing of the cyclotron were recorded for each event.

To determine the level structure of ^{174}W, coincidence cubes were generated and analyzed using INCUB8R and LEVIT8R [11]. Three cubes with different timing conditions were generated. The first cube contained γ rays which were in prompt coincidence, within $\pm$20 ns of the trigger. The second cube included only those transitions that were delayed by 20 ns or more with respect to the trigger, with an additional requirement that these γ rays be within $\pm$20 ns of each other. This cube was, therefore, dominated by decays out of isomers. The third cube included γ rays that were in coincidence within the entire ($\approx$1 μs) time window. The three different cubes provided clean double-gated coincidence spectra and allowed for the discrimination between transitions which were part of prompt structures and those deexciting the isomeric states. In addition, γ-γ matrices with time conditions similar to those for the cubes were also created and analyzed using ESCL8R [11]. The γ-ray energies, intensities, and branching ratios were determined from the analysis. The half-lives of the observed isomeric states in ^{174}W were deduced from energy-time difference matrices, generated using TSCAN [12], by examining the time difference between the transitions feeding the isomeric state and those depopulating it.

The multipolarity of the transitions was obtained from a directional correlation of oriented states (DCO) analysis [13,14], using angle-sorted γ-γ matrices. In order to improve statistics, the γ-ray spectra from detectors clustered at forward and backward angles (17°, 32°, 37°, 143°, 148°, and 163° with respect to the beam axis) were added to form a single spectrum, as were those clustered at angles near 90° (79°, 81°, 90°, 99°, and 101° with respect to the beam axis). The DCO ratios were obtained by determining the areas of the peaks in each of the spectra and taking the ratio of the first ($\approx$30° or 150°) to the second ($\approx$90°). These ratios were normalized to a value of 1.0 for known stretched quadrupole transitions. With this normalization, stretched dipoles yielded a ratio of 0.5, while for ($I \rightarrow I$) transitions, ratios ranging between 1.0 ± 0.2 were obtained.

III. RESULTS

The detailed level scheme of ^{174}W deduced from this work is now extended from about 50 to over 300 assigned transitions and is given in Figs. 1–3. The previously known yrast band and bands 3 and 4 [7] have been extended to higher spin. The *g*- and *s*-band crossings have been firmly established through the observation of non-yrast states on both the high and low sides of the crossing region. A total of 20 bands have been established, a majority of which are assigned as 2-qp excitations. Most of the transitions in band 2, as well as all bands from 5 to 20, are observed here for the first time. The isomeric state reported in previous work [7] is assigned a spin. A new value of its half-life is presented, and the observed band built upon it is discussed. A new, $K^\pi = 12^+$, 4-qp isomer with a rotational band built upon it is observed as well. The energies and intensities of the observed γ rays are shown in Table I, along with the excitation energies and spin assignments for the relevant levels and the DCO ratios for selected in-band and out-of-band transitions.

A. Bands 1 and 2

The *g* band (band 1) has been extended beyond the *g*-*s* band crossing at $I \approx 16\hbar$ up to a spin of $I = 22\hbar$. The *s* band (band 2), has been established from a spin of $I = 8\hbar$ to $I = 26\hbar$, and all transitions are new except the 629-keV line. Band 1 remains yrast till a spin of $16\hbar$, while band 2 becomes favored in energy at higher spins. A number of transitions linking these two bands have been observed in the spin region $I = 8$–$18\hbar$. The DCO ratios of the in-band γ rays that are part of band 2 as well as the high-energy linking transitions between bands 2 and 1 are characteristic of quadrupole transitions and are most probably of electric quadrupole (*E*2) character. The transitions that deexcite the yrast states in bands 1 and 2 are displayed in Fig. 4.

B. Bands 3 and 4

The previously known negative parity band 3 [7,15] has been extended from a spin of 18^- to 24^-, while band 4 has been extended from 19^- to 29^-. These sequences are observed to have strong out-of-band decays at low spins to band 1. Several new transitions connecting bands 3 and 4 are observed. The in-band lines in these two bands are presented in Fig. 5. The spins of the levels in these two bands have been firmly established using the DCO analysis. The 759-, 860- and 970-keV transitions from band 4 to band 1 all have DCO ratios characteristic of stretched dipoles. The 824- and 922-keV transitions from band 3 to band 1 have DCO ratios corresponding to either quadrupoles or ($I \rightarrow I$) transitions. A quadrupole character for these transitions is not indicated by the observed decay pattern between levels in bands 3 and 4, since the linking transitions are much more likely to be $\Delta I = 1$ rather than $\Delta I = 3$. Further, if the 824- and 922-keV transitions were quadrupole in nature, one would expect to also observe the $I \rightarrow I$ transitions, which are not seen. These arguments, combined with the DCO ratios observed for some of the in-band transitions in bands 3 and 4, strongly support the assigned spins. The negative parity assignment is based on conversion coefficient measurements and systematics, as described in earlier work [7]. Further, if band 3 had positive parity, one would have expected to observe *E*2 transitions linking the spin *I* states in band 3 and (*I*-2) levels in band 1, in addition to the $I \rightarrow I$ transitions.

TABLE I. Energies and intensities of γ rays and level energies and spins of initial and final levels in ^{174}W. DCO ratios for a few selected transitions are also given.

E_γ (keV)	E_i (keV)	Band$_i$ $\rightarrow$ Band$_f$	$I_i^\pi \rightarrow I_f^\pi$	I_γ	DCO ratio
101.5(2)	2021	8 $\rightarrow$ 7	$7^- \rightarrow 6^-$	0.44(5)	
112.8(2)	113	1 $\rightarrow$ 1	$2^+ \rightarrow 0^+$	20(3)	
123.8(3)	1919	7 $\rightarrow$ 5	$6^- \rightarrow 6^-$	0.39(3)	
124.0(2)	2145	7 $\rightarrow$ 8	$8^- \rightarrow 7^-$	0.52(7)	
135.3(2)	3529	2 $\rightarrow$ 1	$16^+ \rightarrow 16^+$	0.24(4)	
144.9(4)	3386	4 $\rightarrow$ 3	$15^- \rightarrow 14^-$	–	
145.1(2)	2290	8 $\rightarrow$ 7	$9^- \rightarrow 8^-$	0.72(7)	
169.0(3)	3965	4 $\rightarrow$ 3	$17^- \rightarrow 16^-$	–	
170.0(2)	2065	5 $\rightarrow$ 6	$8^- \rightarrow 7^-$	0.21(3)	
174.8(2)	2465	7 $\rightarrow$ 8	$10^- \rightarrow 9^-$	0.65(6)	
183.1(2)	2648	8 $\rightarrow$ 7	$11^- \rightarrow 10^-$	0.70(6)	
192.5(4)	3526	6 $\rightarrow$ 7	$15^- \rightarrow 14^-$	–	
197.1(2)	1627	3 $\rightarrow$ 5$^-$	$6^- \rightarrow 5^{(-)}$	0.85(6)	
199.0(2)	3715	18 $\rightarrow$ 17	$13^+ \rightarrow 12^+$	0.84(8)	
200.8(2)	4176	1 $\rightarrow$ 2	$18^+ \rightarrow 18^+$	0.48(6)	
206.7(2)	2395	4 $\rightarrow$ 1	$11^- \rightarrow 12^+$	0.62(6)	
206.7(2)	2855	7 $\rightarrow$ 8	$12^- \rightarrow 11^-$	1.24(8)	
214.0(2)	1919	7 $\rightarrow$ 5$^-$	$6^- \rightarrow 5^{(-)}$	0.92(7)	0.46(4)
216.2(2)	3931	17 $\rightarrow$ 18	$14^+ \rightarrow 13^+$	0.73(6)	
219.6(2)	2487	16 $\rightarrow$ 15	$9^- \rightarrow 8^-$	1.64(9)	
222.0(2)	2183	6 $\rightarrow$ 3	$9^- \rightarrow 8^-$	0.10(2)	
224.6(2)	2553	6 $\rightarrow$ 3	$11^- \rightarrow 10^-$	0.65(5)	
225.2(4)	3055	20 $\rightarrow$ 19	11 $\rightarrow$ 10	–	
225.6(4)	2145	7 $\rightarrow$ 7	$8^- \rightarrow 6^-$	–	
226.7(2)	1627	3 $\rightarrow$ 4	$6^- \rightarrow 5^-$	0.14(3)	
230.5(2)	2718	15 $\rightarrow$ 16	$10^- \rightarrow 9^-$	1.06(6)	
232.8(2)	4163	18 $\rightarrow$ 17	$15^+ \rightarrow 14^+$	0.64(6)	
235.8(3)	4117	6 $\rightarrow$ 7	$17^- \rightarrow 16^-$	–	
238.3(2)	3333	7 $\rightarrow$ 8	$14^- \rightarrow 13^-$	0.67(5)	
239.7(2)	3095	8 $\rightarrow$ 7	$13^- \rightarrow 12^-$	0.98(6)	
240.7(2)	2958	16 $\rightarrow$ 15	$11^- \rightarrow 10^-$	1.04(7)	
241.0(3)	3296	19 $\rightarrow$ 20	12 $\rightarrow$ 11	–	
241.4(3)	3271	12 $\rightarrow$ 13	13 $\rightarrow$ 12$^{(+)}$	–	
243.2(2)	356	1 $\rightarrow$ 1	$4^+ \rightarrow 2^+$	100(3)	
244.8(2)	1675	4 $\rightarrow$ 5$^-$	$7^- \rightarrow 5^{(-)}$	1.41(11)	
247.0(2)	2268	15 $\rightarrow$ 8	$8^- \rightarrow 7^-$	1.44(9)	0.48(4)
249.0(2)	1919	7 $\rightarrow$ 5$^-$	$6^- \rightarrow 5^{(-)}$	0.65(5)	
249.3(2)	4412	17 $\rightarrow$ 18	$16^+ \rightarrow 15^+$	0.60(7)	
250.4(2)	3209	15 $\rightarrow$ 16	$12^- \rightarrow 11^-$	1.01(6)	
252.7(2)	3003	6 $\rightarrow$ 3	$13^- \rightarrow 12^-$	0.47(4)	
254.4(3)	3551	20 $\rightarrow$ 19	13 $\rightarrow$ 12	–	
258.1(2)	3881	7 $\rightarrow$ 8	$16^- \rightarrow 15^-$	0.44(5)	
258.4(3)	3747	12 $\rightarrow$ 13	15 $\rightarrow$ 14$^{(+)}$	–	
261.1(2)	3470	16 $\rightarrow$ 15	$13^- \rightarrow 12^-$	0.80(6)	
263.3(2)	1627	3 $\rightarrow$ 3	$6^- \rightarrow 4^-$	1.79(8)	
264.4(2)	3046	2 $\rightarrow$ 1	$14^+ \rightarrow 14^+$	1.06(7)	
264.6(2)	2448	5 $\rightarrow$ 6	$10^- \rightarrow 9^-$	0.28(4)	
265.1(2)	4677	18 $\rightarrow$ 17	$17^+ \rightarrow 16^+$	0.51(6)	
268.7(2)	2290	8 $\rightarrow$ 8	$9^- \rightarrow 7^-$	0.39(5)	
270.2(1)	2065	5 $\rightarrow$ 5	$8^- \rightarrow 6^-$	0.43(4)	
270.6(4)	3822	19 $\rightarrow$ 20	14 $\rightarrow$ 13	–	
272.2(2)	3742	15 $\rightarrow$ 16	$14^- \rightarrow 13^-$	0.65(5)	
274.6(2)	1675	4 $\rightarrow$ 4	$7^- \rightarrow 5^-$	0.51(6)	
277.7(2)	3324	9 $\rightarrow$ 2	$14^+ \rightarrow 14^+$	0.34(4)	0.98(6)
278.2(4)	4100	20 $\rightarrow$ 19	15 $\rightarrow$ 14	–	
278.4(2)	2926	5 $\rightarrow$ 8	$12^- \rightarrow 11^-$	0.51(5)	

TABLE I. (*Continued*.)

E_γ (keV)	E_i (keV)	Band$_i$ → Band$_f$	$I_i^\pi \rightarrow I_f^\pi$	I_γ	DCO ratio
279.7(2)	2109	12 → 12	$7 \rightarrow 5$	0.19(5)	
280.3(2)	4957	17 → 18	$18^+ \rightarrow 17^+$	0.46(5)	
281.7(3)	4268	12 → 13	$17 \rightarrow 16^{(+)}$	–	
284.1(2)	4026	16 → 15	$15^- \rightarrow 14^-$	0.55(5)	
285.8(2)	3526	6 → 3	$15^- \rightarrow 14^-$	0.16(3)	
286.2(2)	1962	3 → 4	$8^- \rightarrow 7^-$	0.54(5)	
288.4(2)	2183	6 → 6	$9^- \rightarrow 7^-$	3.16(14)	
289.4(2)	3623	8 → 7	$15^- \rightarrow 14^-$	0.61(6)	
294.7(2)	5252	18 → 17	$19^+ \rightarrow 18^+$	0.39(4)	
297.0(2)	4323	15 → 16	$16^- \rightarrow 15^-$	0.39(4)	
299.2(4)	4485	7 → 8	$18^- \rightarrow 17^-$	–	
301.0(2)	2488	9 → 1	$10^+ \rightarrow 12^+$	0.16(3)	
301.7(2)	3831	9 → 2	$16^+ \rightarrow 16^+$	0.25(5)	
302.9(2)	2448	5 → 7	$10^- \rightarrow 8^-$	0.16(3)	
303.1(2)	3211	10 → 10	$13 \rightarrow 11$	0.21(5)	
305.0(3)	4186	8 → 7	$17^- \rightarrow 16^-$	–	
306.8(2)	3516	17 → 15	$12^+ \rightarrow 12^-$	0.16(3)	
306.8(4)	4407	19 → 20	$16 \rightarrow 15$	–	
308.4(2)	4632	16 → 15	$17^- \rightarrow 16^-$	0.32(4)	
309.3(2)	5561	17 → 18	$20^+ \rightarrow 19^+$	0.35(4)	
311.6(2)	3637	10 → 9	$15 \rightarrow 14^+$	0.10(3)	
319.8(2)	2465	7 → 7	$10^- \rightarrow 8^-$	0.72(5)	
320.4(2)	2648	8 → 3	$11^- \rightarrow 10^-$	0.17(3)	
322.4(1)	1998	4 → 4	$9^- \rightarrow 7^-$	3.93(15)	
322.7(3)	5884	18 → 17	$21^+ \rightarrow 20^+$	0.27(4)	
323.3(2)	4955	15 → 16	$18^- \rightarrow 17^-$	0.28(4)	
328.4(2)	2290	8 → 3	$9^- \rightarrow 8^-$	0.19(3)	
329.9(2)	2328	3 → 4	$10^- \rightarrow 9^-$	0.41(4)	
330.4(2)	3333	7 → 6	$14^- \rightarrow 13^-$	0.37(4)	
332.1(3)	5287	16 → 15	$19^- \rightarrow 18^-$	0.19(4)	
334.2(2)	1962	3 → 3	$8^- \rightarrow 6^-$	5.10(18)	1.01(2)
335.1(3)	4167	10 → 9	$17 \rightarrow 16^+$	0.12(3)	
338.4(4)	6222	17 → 18	$22^+ \rightarrow 21^+$	0.15(5)	
341.7(3)	2451	12 → 12	$9 \rightarrow 7$	0.67(6)	
349.1(2)	705	1 → 1	$6^+ \rightarrow 4^+$	84(3)	
353.4(3)	3448	5 → 8	$14^- \rightarrow 13^-$	0.50(8)	
354.2(3)	2750	3 → 4	$12^- \rightarrow 11^-$	0.28(4)	
354.9(3)	3881	7 → 6	$16^- \rightarrow 15^-$	0.26(5)	
358.1(2)	2648	8 → 8	$11^- \rightarrow 9^-$	1.48(7)	
361.1(3)	1998	4 → 1	$9^- \rightarrow 10^+$	1.37(7)	
366.4(2)	2328	3 → 3	$10^- \rightarrow 8^-$	3.90(14)	
368.7(3)	4485	7 → 6	$18^- \rightarrow 17^-$	0.19(4)	
370.4(2)	2553	6 → 6	$11^- \rightarrow 9^-$	4.95(18)	
378.2(3)	2866	9 → 9	$12^+ \rightarrow 10^+$	0.26(3)	
379.8(4)	3240	3 → 4	$14^- \rightarrow 13^-$	–	
380.0(3)	2375	14 → 14		0.29(3)	
383.2(2)	2448	5 → 5	$10^- \rightarrow 8^-$	1.21(9)	
389.8(2)	2855	7 → 7	$12^- \rightarrow 10^-$	1.81(7)	
395.4(3)	4018	5 → 8	$16^- \rightarrow 15^-$	0.25(6)	
396.8(3)	2848	12 → 12	$11 \rightarrow 9$	1.12(8)	
397.2(2)	2395	4 → 4	$11^- \rightarrow 9^-$	8.4(3)	
399.7(3)	2465	7 → 5	$10^- \rightarrow 8^-$	1.52(8)	
401.0(3)	3211	10 → 11	$13 \rightarrow 11$	0.77(6)	
402.0(3)	3046	2 → 2	$14^+ \rightarrow 12^+$	1.14(7)	
404.7(3)	1853	11 → 11	$7 \rightarrow 5$	0.36(6)	
406.2(2)	2855	7 → 5	$12^- \rightarrow 10^-$	1.78(8)	
406.6(3)	3333	7 → 5	$14^- \rightarrow 12^-$	0.68(6)	

TABLE I. (*Continued*.)

E_γ (keV)	E_i (keV)	Band$_i$ → Band$_f$	$I_i^\pi \rightarrow I_f^\pi$	I_γ	DCO ratio
410.7(4)	3797	3 → 4	$16^- \rightarrow 15^-$	–	
411.9(3)	2787	14 → 14		0.49(6)	
415.3(4)	3931	17 → 17	$14^+ \rightarrow 12^+$	0.12(5)	
415.8(2)	2644	2 → 2	$12^+ \rightarrow 10^+$	1.12(6)	
421.4(2)	2750	3 → 3	$12^- \rightarrow 10^-$	3.59(13)	
422.6(3)	3271	12 → 12	13 → 11	1.31(8)	
426.3(3)	3637	10 → 10	15 → 13	1.02(6)	
427.6(3)	3211	10 → 1	13 → 14^+	0.46(6)	
431.3(3)	1794	5 → 3	$6^- \rightarrow 4^-$	1.23(10)	
432.7(2)	1138	1 → 1	$8^+ \rightarrow 6^+$	56(2)	
432.9(4)	3881	7 → 5	$16^- \rightarrow 14^-$	0.26(5)	
438.4(2)	2065	5 → 3	$8^- \rightarrow 6^-$	1.42(12)	
440.9(3)	2229	2 → 2	$10^+ \rightarrow 8^+$	1.14(10)	
443.9(3)	3973	2 → 2	$18^+ \rightarrow 16^+$	0.72(6)	
446.7(2)	3095	8 → 8	$13^- \rightarrow 11^-$	2.86(9)	
448.2(4)	4163	18 → 18	$15^+ \rightarrow 13^+$	0.26(4)	
449.4(2)	3003	6 → 6	$13^{(-)} \rightarrow 11^{(-)}$	4.72(20)	
450.2(3)	3237	14 → 14		0.69(7)	
450.5(3)	2718	15 → 15	$10^{(-)} \rightarrow 8^{(-)}$	0.26(4)	
451.0(3)	3687	14 → 14		0.59(7)	
452.0(4)	4427	9 → 2	$(18^+) \rightarrow (18^+)$	–	
457.2(3)	2644	2 → 1	$12^+ \rightarrow 12^+$	0.97(11)	
458.4(3)	3324	9 → 9	$14^+ \rightarrow 12^+$	0.43(5)	
458.6(3)	3489	13 → 13	$14^{(+)} \rightarrow 12^{(+)}$	0.62(6)	
459.4(3)	3271	12 → 11	13 → 11	0.96(6)	
460.4(3)	2313	11 → 11	9 → 7	0.52(5)	
461.3(2)	2926	5 → 7	$12^- \rightarrow 10^-$	1.24(8)	
465.0(2)	2860	4 → 4	$13^- \rightarrow 11^-$	10.0(3)	0.98(2)
466.6(5)	3296	19 → 19	12 → 10	–	
467.0(4)	4485	7 → 5	$18^- \rightarrow 16^-$	–	
470.9(3)	2958	16 → 16	$11^- \rightarrow 9^-$	0.43(4)	
476.4(2)	3747	12 → 12	15 → 13	1.78(10)	
477.6(2)	2926	5 → 5	$12^- \rightarrow 10^-$	1.71(10)	
478.2(2)	3333	7 → 7	$14^- \rightarrow 12^-$	2.66(12)	
482.6(3)	4412	17 → 17	$16^+ \rightarrow 14^+$	0.31(4)	
482.8(3)	3529	2 → 2	$16^+ \rightarrow 14^+$	0.80(8)	
487.2(2)	2448	5 → 3	$10^- \rightarrow 8^-$	1.05(6)	
490.7(2)	3240	3 → 3	$14^- \rightarrow 12^-$	3.16(11)	
490.9(3)	3209	15 → 15	$12^- \rightarrow 10^-$	0.55(5)	
495.4(5)	3551	20 → 20	13 → 11	–	
495.4(3)	1895	6 → 4	$7^- \rightarrow 5^-$	0.52(6)	
497.1(3)	3986	13 → 13	$16^{(+)} \rightarrow 14^{(+)}$	0.90(8)	
497.4(3)	2811	11 → 11	11 → 9	0.72(10)	
498.5(2)	1636	1 → 1	$10^+ \rightarrow 8^+$	37(1)	
499.9(3)	4187	14 → 14		0.57(7)	
503.7(2)	2465	7 → 3	$10^- \rightarrow 8^-$	0.85(6)	
506.9(2)	3831	9 → 9	$16^+ \rightarrow 14^+$	1.40(8)	
508.5(4)	2183	6 → 4	$9^- \rightarrow 7^-$	0.17(3)	
511.0(3)	3470	16 → 16	$13^- \rightarrow 11^-$	0.66(6)	
514.2(3)	4677	18 → 18	$17^+ \rightarrow 15^+$	0.41(5)	
520.9(3)	4268	12 → 12	17 → 15	1.43(8)	
522.3(2)	3448	5 → 5	$14^- \rightarrow 12^-$	2.31(12)	
523.4(2)	3526	6 → 6	$15^- \rightarrow 13^-$	4.39(18)	
525.2(5)	3822	19 → 19	14 → 12	–	
525.8(2)	3386	4 → 4	$15^- \rightarrow 13^-$	8.6(3)	
528.4(2)	3623	8 → 8	$15^- \rightarrow 13^-$	3.80(15)	
529.7(2)	4167	10 → 10	17 → 15	1.76(10)	

TABLE I. (*Continued*.)

E_γ (keV)	E_i (keV)	Band$_i$ → Band$_f$	$I_i^\pi \rightarrow I_f^\pi$	I_γ	DCO ratio
533.9(3)	3742	15 → 15	$14^- \rightarrow 12^-$	0.85(7)	
535.0(3)	2848	12 → 11	$11 \rightarrow 9$	0.83(9)	
536.8(3)	4724	14 → 14		0.43(7)	
537.0(2)	1675	4 → 1	$7^- \rightarrow 8^+$	2.33(17)	
537.4(2)	4723	8 → 8	$19^- \rightarrow 17^-$	1.18(14)	
540.7(3)	4527	13 → 13	$18^{(+)} \rightarrow 16^{(+)}$	0.53(8)	
541.6(2)	3095	8 → 6	$13^- \rightarrow 11^-$	1.73(9)	
545.7(2)	4957	17 → 17	$18^+ \rightarrow 16^+$	0.50(6)	
547.0(3)	2183	6 → 1	$9^- \rightarrow 10^+$	0.37(6)	
547.9(2)	3881	7 → 7	$16^- \rightarrow 14^-$	3.16(13)	
549.0(4)	4100	20 → 20	$15 \rightarrow 13$	–	
551.7(2)	2188	1 → 1	$12^+ \rightarrow 10^+$	27.8(9)	
555.2(2)	2553	6 → 4	$11^- \rightarrow 9^-$	1.20(11)	
556.1(2)	3797	3 → 3	$16^- \rightarrow 14^-$	2.64(10)	
556.9(3)	4026	16 → 16	$15^- \rightarrow 13^-$	0.73(8)	
557.1(4)	3516	17 → 16	$12^+ \rightarrow 11^-$	–	
563.8(2)	4186	8 → 8	$17^- \rightarrow 15^-$	1.83(11)	
563.9(4)	5288	14 → 14		0.21(5)	
565.4(4)	3211	10 → 2	$13 \rightarrow 12^+$	0.19(4)	
570.1(2)	4018	5 → 5	$16^- \rightarrow 14^-$	1.46(9)	
572.4(2)	4840	12 → 12	$19 \rightarrow 17$	1.09(7)	
575.1(3)	5252	18 → 18	$19^+ \rightarrow 17^+$	0.42(5)	
579.7(2)	3965	4 → 4	$17^- \rightarrow 15^-$	8.1(3)	
580.3(3)	3973	2 → 1	$18^+ \rightarrow 16^+$	6.81(24)	0.94(3)
581.8(3)	4323	15 → 15	$16^{(-)} \rightarrow 14^{(-)}$	0.62(7)	
585.0(5)	4407	19 → 19	$16 \rightarrow 14$	–	
590.0(3)	3637	10 → 2	$15^{(+)} \rightarrow 14^+$	0.42(7)	
590.8(4)	3986	13 → 1	$16^{(+)} \rightarrow 16^+$	0.14(4)	
591.2(2)	4117	6 → 6	$17^{(-)} \rightarrow 15^{(-)}$	3.08(14)	
594.2(2)	2229	2 → 1	$10^+ \rightarrow 10^+$	2.32(14)	
594.5(2)	4427	9 → 9	$18^+ \rightarrow 16^+$	1.12(8)	
595.0(4)	2908	10 → 11	$11 \rightarrow 9$	0.10(1)	
595.8(2)	2783	1 → 1	$14^+ \rightarrow 12^+$	20.5(7)	
598.0(3)	4616	5 → 5	$18^- \rightarrow 16^-$	1.10(13)	
598.2(3)	2926	5 → 3	$12^- \rightarrow 10^-$	0.62(6)	
598.2(4)	2451	12 → 11	$9 \rightarrow 7$	0.06(2)	
601.0(3)	5441	12 → 12	$21 \rightarrow 19$	0.91(7)	
602.0(2)	3386	4 → 1	$15^- \rightarrow 14^+$	1.45(10)	
604.0(3)	5561	17 → 17	$20^+ \rightarrow 18^+$	0.50(5)	
604.1(2)	4485	7 → 7	$18^- \rightarrow 16^-$	4.35(17)	
605.4(3)	4632	16 → 16	$17^- \rightarrow 15^-$	0.54(6)	
608.1(2)	3003	6 → 4	$13^- \rightarrow 11^-$	1.65(14)	
611.8(2)	3395	1 → 1	$16^+ \rightarrow 14^+$	13.6(4)	
613.1(3)	5229	5 → 5	$20^- \rightarrow 18^-$	0.65(8)	
615.6(2)	4412	3 → 3	$18^- \rightarrow 16^-$	2.07(11)	
615.7(2)	5201	4 → 4	$21^- \rightarrow 19^-$	3.59(14)	
619.6(2)	3623	8 → 6	$15^- \rightarrow 13^-$	2.24(15)	
620.0(2)	4585	4 → 4	$19^- \rightarrow 17^-$	5.50(20)	
620.2(2)	4787	10 → 10	$19 \rightarrow 17$	1.38(13)	
620.4(3)	5344	8 → 8	$21^- \rightarrow 19^-$	0.88(8)	
622.8(3)	2811	11 → 1	$11 \rightarrow 12^+$	0.20(4)	
628.9(2)	4602	2 → 2	$20^+ \rightarrow 18^+$	4.48(17)	
631.1(3)	4955	15 → 15	$18^- \rightarrow 16^-$	0.47(6)	
631.6(3)	5884	18 → 18	$21^+ \rightarrow 19^+$	0.44(5)	
631.6(3)	5059	9 → 9	$20^+ \rightarrow 18^+$	0.83(6)	
632.4(2)	5833	4 → 4	$23^- \rightarrow 21^-$	1.64(8)	
640.4(2)	5126	7 → 7	$20^- \rightarrow 18^-$	2.05(11)	

TABLE I. (*Continued*.)

E_γ (keV)	E_i (keV)	Band$_i$ → Band$_f$	$I_i^\pi \rightarrow I_f^\pi$	I_γ	DCO ratio
642.3(2)	5871	5 → 5	$22^- \rightarrow 20^-$	0.43(7)	
645.6(3)	4176	1 → 2	$18^+ \rightarrow 16^+$	1.37(11)	
646.7(2)	5706	9 → 9	$22^+ \rightarrow 20^+$	0.49(8)	
651.2(3)	1788	2 → 1	$8^+ \rightarrow 8^+$	0.68(12)	
652.3(2)	4770	6 → 6	$19^- \rightarrow 17^-$	1.82(11)	
654.8(3)	5442	10 → 10	$21 \rightarrow 19$	0.86(9)	
655.4(4)	5287	16 → 16	$19^- \rightarrow 17^-$	0.34(5)	
660.1(4)	2848	12 → 1	$11 \rightarrow 12^+$	–	
660.7(5)	2109	12 → 11	$7 \rightarrow 5$	–	
661.0(4)	4186	8 → 6	$17^- \rightarrow 15^-$	0.10(1)	
661.1(4)	6222	17 → 17	$22^+ \rightarrow 20^+$	0.32(5)	
665.8(3)	3526	6 → 4	$15^- \rightarrow 13^-$	0.51(7)	
667.4(2)	5793	7 → 7	$22^- \rightarrow 20^-$	1.16(9)	
670.3(2)	5083	3 → 3	$20^- \rightarrow 18^-$	1.37(8)	
672.1(3)	2860	4 → 1	$13^- \rightarrow 12^+$	0.93(9)	
674.0(3)	6115	12 → 12	$23 \rightarrow 21$	0.58(7)	
674.8(3)	6117	10 → 10	$23 \rightarrow 21$	0.62(8)	
676.7(3)	2313	11 → 1	$9 \rightarrow 10^+$	0.46(8)	
679.7(3)	3324	9 → 2	$14^+ \rightarrow 12^+$	0.48(7)	
680.0(3)	2866	9 → 1	$12^+ \rightarrow 12^+$	0.67(11)	
681.1(4)	5636	15 → 15	$20^- \rightarrow 18^-$	0.23(5)	
685.6(5)	3516	17 → 19	$12^+ \rightarrow 10$	–	
687.4(4)	6571	18 → 18	$23^+ \rightarrow 21^+$	0.16(4)	
692.4(3)	2328	3 → 1	$10^- \rightarrow 10^+$	0.55(7)	
693.5(4)	5981	16 → 16	$21^- \rightarrow 19^-$	0.17(5)	
695.1(2)	1400	4 → 1	$5^- \rightarrow 6^+$	2.29(21)	
701.7(2)	5472	6 → 6	$21^- \rightarrow 19^-$	1.38(9)	
702.4(3)	6535	4 → 4	$25^- \rightarrow 23^-$	1.05(7)	
703.8(3)	6497	7 → 7	$24^- \rightarrow 22^-$	0.90(8)	
705.6(4)	3489	13 → 1	$14^{(+)} \rightarrow 14^+$	0.49(7)	
706.2(2)	5308	2 → 2	$22^+ \rightarrow 20^+$	2.62(10)	
715.1(3)	1853	11 → 1	$7 \rightarrow 8^+$	0.31(5)	
721.8(2)	5805	3 → 3	$22^- \rightarrow 20^-$	0.81(6)	
724.0(3)	6841	10 → 10	$25 \rightarrow 23$	0.32(6)	
724.1(3)	6196	6 → 6	$23^- \rightarrow 21^-$	0.68(10)	
724.2(3)	1430	5^- → 1	$5^{(-)} \rightarrow 6^+$	0.82(8)	
727.0(2)	4903	1 → 1	$20^+ \rightarrow 18^+$	1.47(12)	
731.6(3)	4117	6 → 4	$17^- \rightarrow 15^-$	0.27(5)	
738.4(3)	2926	5 → 1	$12^- \rightarrow 12^+$	0.80(10)	
738.7(4)	2375	14 → 1	$\rightarrow 10^+$	0.18(5)	
742.9(3)	1448	11 → 1	$5 \rightarrow 6^+$	0.25(4)	
743.5(3)	6450	9 → 9	$24^+ \rightarrow 22^+$	0.23(6)	
746.6(3)	7244	7 → 7	$26^- \rightarrow 24^-$	0.48(6)	
747.4(2)	3529	2 → 1	$16^+ \rightarrow 14^+$	3.45(17)	0.94(4)
753.1(2)	5656	1 → 1	$22^+ \rightarrow 20^+$	0.67(9)	
757.1(3)	1895	6 → 1	$7^- \rightarrow 8^+$	0.68(7)	
758.7(3)	2395	4 → 1	$11^- \rightarrow 10^+$	4.38(17)	0.58(3)
771.8(3)	4167	10 → 1	$17 \rightarrow 16^+$	0.35(6)	
772.9(3)	6578	3 → 3	$24^- \rightarrow 22^-$	0.44(8)	
778.0(2)	6086	2 → 2	$24^+ \rightarrow 22^+$	1.75(8)	
780.7(2)	7316	4 → 4	$27^- \rightarrow 25^-$	0.78(8)	
780.9(2)	4176	1 → 1	$18^+ \rightarrow 16^+$	2.59(14)	
784.7(2)	3831	9 → 2	$16^+ \rightarrow 14^+$	0.95(8)	
811.6(3)	2448	5 → 1	$10^- \rightarrow 10^+$	0.94(11)	
814.1(3)	3003	6 → 1	$13^- \rightarrow 12^+$	0.94(11)	
814.7(4)	2451	12 → 1	$9 \rightarrow 10^+$	–	
823.7(2)	1962	3 → 1	$8^- \rightarrow 8^+$	1.62(11)	1.06(4)

TABLE I. (*Continued*.)

E_γ (keV)	E_i (keV)	Band$_i$ → Band$_f$	$I_i^\pi \rightarrow I_f^\pi$	I_γ	DCO ratio
842.1(3)	3030	13 → 1	$12^{(+)} \rightarrow 12^+$	0.43(6)	
842.7(3)	6929	2 → 2	$26^+ \rightarrow 24^+$	0.74(12)	
847.3(3)	8164	4 → 4	$29^- \rightarrow 27^-$	0.56(7)	
853.9(3)	3637	10 → 1	$15 \rightarrow 14^+$	0.32(6)	
857.1(4)	1995	14 → 1	$\rightarrow 8^+$	0.14(4)	
859.7(3)	1998	4 → 1	$9^- \rightarrow 8^+$	6.3(3)	0.55(2)
860.4(3)	3046	2 → 1	$14^+ \rightarrow 12^+$	2.98(21)	0.85(4)
897.4(3)	4427	9 → 2	$18^+ \rightarrow 16^+$	0.85(12)	0.95(5)
916.7(3)	2553	6 → 1	$11^- \rightarrow 10^+$	2.48(18)	0.47(2)
922.0(3)	1627	3 → 1	$6^- \rightarrow 6^+$	4.57(23)	1.00(2)
927.6(3)	2065	5 → 1	$8^- \rightarrow 8^+$	0.74(9)	0.96(4)
964.7(3)	1670	5^- → 1	$5^{(-)} \rightarrow 6^+$	0.52(7)	0.55(4)
970.1(3)	1675	4 → 1	$7^- \rightarrow 6^+$	2.63(20)	0.50(2)
971.1(5)	2109	12 → 1	$7 \rightarrow 8^+$	–	
999.7(3)	1705	5^- → 1	$5^{(-)} \rightarrow 6^+$	0.81(10)	0.63(4)
1007.7(3)	1364	3 → 1	$4^- \rightarrow 4^+$	2.0(3)	0.95(4)
1010.0(3)	2644	2 → 1	$12^+ \rightarrow 10^+$	1.23(11)	0.93(6)
1023.1(4)	3211	10 → 1	$13 \rightarrow 12^+$	0.22(5)	0.57(5)
1044.6(3)	1400	4 → 1	$5^- \rightarrow 4^+$	4.1(4)	
1045.3(4)	2183	6 → 1	$9^- \rightarrow 8^+$	1.32(9)	0.46(4)
1073.9(5)	1430	5^- → 1	$5^{(-)} \rightarrow 4^+$	0.14(4)	
1089.9(3)	1794	5 → 1	$6^- \rightarrow 6^+$	1.90(17)	0.99(5)
1091.9(6)	2229	2 → 1	$10^+ \rightarrow 8^+$	–	
1092.0(5)	1448	11 → 1	$5 \rightarrow 4^+$	0.10(4)	
1147.9(4)	1853	11 → 1	$7 \rightarrow 6^+$	0.55(5)	0.49(6)
1174.8(4)	2811	11 → 1	$11 \rightarrow 10^+$	1.35(9)	0.54(5)
1175.9(4)	2313	11 → 1	$9 \rightarrow 8^+$	1.11(12)	0.64(4)
1190.0(4)	1895	6 → 1	$7^- \rightarrow 6^+$	0.72(5)	0.51(5)
1193.7(4)	2830	19 → 1	$10 \rightarrow 10^+$	0.30(6)	0.91(9)
1202.6(5)	3986	13 → 1	$16^{(+)} \rightarrow 14^+$	0.20(5)	
1211.7(5)	2848	12 → 1	$11 \rightarrow 10^+$	0.57(8)	0.55(6)
1237.1(3)	2375	14 → 1	$\rightarrow 8^+$	0.20(4)	
1271.7(4)	2908	10 → 1	$11 \rightarrow 10^+$	0.08(3)	0.54(7)
1289.9(5)	1995	14 → 1	$\rightarrow 6^+$	0.17(4)	
1301.1(4)	3489	13 → 1	$14^{(+)} \rightarrow 12^+$	0.32(5)	
1313.1(4)	2451	12 → 1	$9 \rightarrow 8^+$	0.20(5)	0.58(8)
1314.2(5)	1670	5^- → 1	$5^{(-)} \rightarrow 4^+$	0.21(5)	0.52(6)
1327.7(4)	3516	17 → 1	$12^+ \rightarrow 12^+$	0.26(3)	0.91(8)
1349.1(4)	1705	5^- → 1	$5^{(-)} \rightarrow 4^+$	0.26(6)	0.64(7)
1393.7(4)	3030	13 → 1	$12^{(+)} \rightarrow 10^+$	0.37(6)	1.01(9)
1403.9(5)	2109	12 → 1	$7 \rightarrow 6^+$	0.18(4)	
1473.0(6)	1829	12 → 1	$5 \rightarrow 4^+$	0.15(3)	
1879.3(5)	3516	17 → 1	$12^+ \rightarrow 10^+$	0.48(6)	0.95(6)

C. Bands 5 and 6

As mentioned above, all bands labeled 5–20 are new. Bands 5 and 6 have been established to spins of 22 and 23 $\hbar$, respectively. These structures have strong decays to bands 1, 3 and 4. The DCO ratios for the 917-, 1045- and 1190-keV transitions de-exciting band 6 to band 1 are consistent with those of stretched dipoles, while the 928- and 1090-keV transitions deexciting band 5 are either of the $I \rightarrow I$ type or stretched quadrupoles. The spin and parity assignments have been obtained using arguments similar to those described for bands 3 and 4, and are also supported by the observed decay patterns to bands 3 and 4.

D. Bands 7 and 8

As can be seen from Fig. 1, bands 7 and 8 form a strongly coupled rotational sequence and have been observed up to spins of 26 and 21 $\hbar$, respectively. These bands do not exhibit strong decays to band 1, unlike the bands described earlier. The out-of-band decay proceeds to bands 5 and 6 as well as to some intrinsic states. The transitions in bands 7 and 8 are shown in Fig. 6. The spin and parity assignments are based on the following arguments. A stretched dipole character is indicated by the measured DCO ratios for the 965-, 1000-, 1314-, and 1349-keV transitions deexciting the two intrinsic $I = 5$ states. Band 7 is observed to decay to one of these states

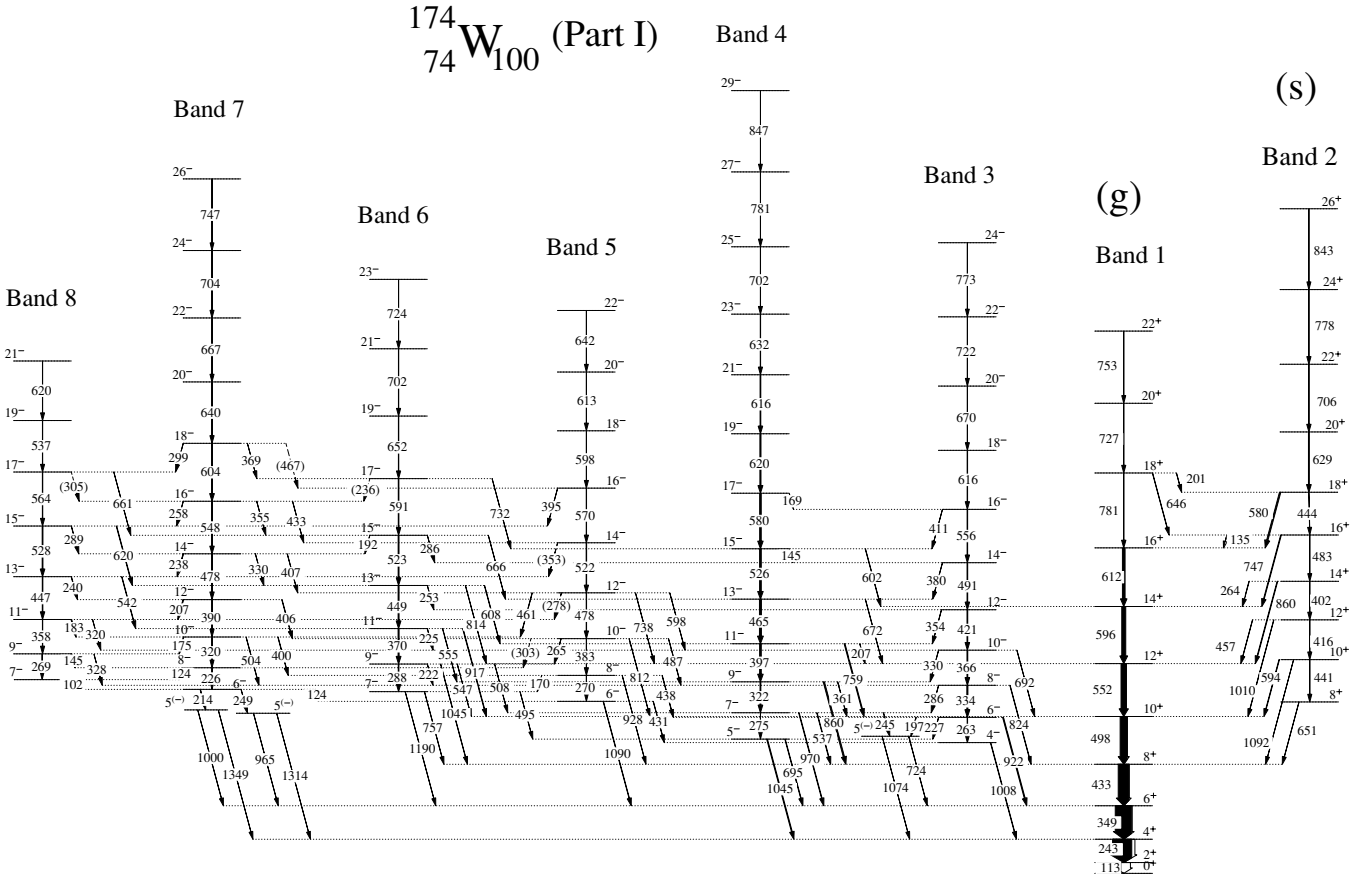

FIG. 1. Level scheme for ^{174}W showing the yrast and $K \leqslant 6$ negative parity bands.

through the 214-keV transition, for which a dipole character is inferred from the DCO ratios. A spin assignment of $I = 6$ for the lowest state in band 7 is, therefore, most probable. The dual transition branches from members of bands 7 and 8 to bands 5 and 6 are most likely to have $M1$ and $E2$ character rather than $E1$ and $M2$ character, from a consideration of comparable transition probabilities. This would indicate negative parity for both bands 7 and 8.

E. Bands 9 to 14

Band 9 has been observed up to a spin of $24\hbar$. The out-of-band decay is predominantly to band 1 below the backbend and band 2 above it. The spin assignment for band 9 is based upon the measured DCO ratios for the 278- and 897-keV γ rays which are consistent with either $I \rightarrow I$ or quadrupole transitions. An assignment of positive parity to band 9 follows from the fact that the 680-, 785-, and 897-keV transitions deexciting toward band 2 are more likely to have an $E2$ than an $M2$ character, given the competing dipole branches.

Band 10 has been observed from a spin of 11 to $25\hbar$, band 11 from 5 to $11\hbar$, and band 12 from 5 to $23\hbar$. Above a spin of $9\hbar$, the intensity from band 11 is seen to branch out with comparable strengths into bands 10 and 12. All three sequences have strong out-of-band decays to band 1 at low spins, while band 10 also decays to band 2 at higher spins in a manner similar to band 9. The transitions deexciting these bands to band 1, viz., the 1023- and 1272-keV transitions from band 10, the 1148-, 1175-, and 1176-keV lines from band 11, and the 1212- and 1313-keV γ rays from band 12, all have DCO ratios consistent with stretched dipole character, indicating the assigned spins. It was not possible to obtain firm parity assignments for these bands from the available experimental information. However, based on the observed decay patterns from bands 10 and 12 to band 11 (the 401- and 595-keV transitions from band 10, and the 459- and 535-keV lines from band 12), the same parity assignment for all three bands appears most likely. This follows from an expected $E2$ as opposed to $M2$ character for the above-mentioned transitions.

Bands 13 and 14 are observed to spins of 18 and $20\hbar$, respectively. In addition to the in-band transitions, these bands deexcite to band 1. The DCO ratio for the 1394-keV transition is consistent with quadrupole or $I \rightarrow I$ nature, indicating an even spin assignment for band 13. The tentative positive parity is based on an $E2$ character for most of the out-of-band decays. It was not possible to assign spins or parities for the states in band 14 based on the available information; therefore, this band will not be discussed subsequently.

F. Bands 15 and 16

Bands 15 and 16 (Fig. 7) are strongly coupled sequences built upon one of the two isomeric states observed in ^{174}W. A few transitions in these bands had been previously reported [7],

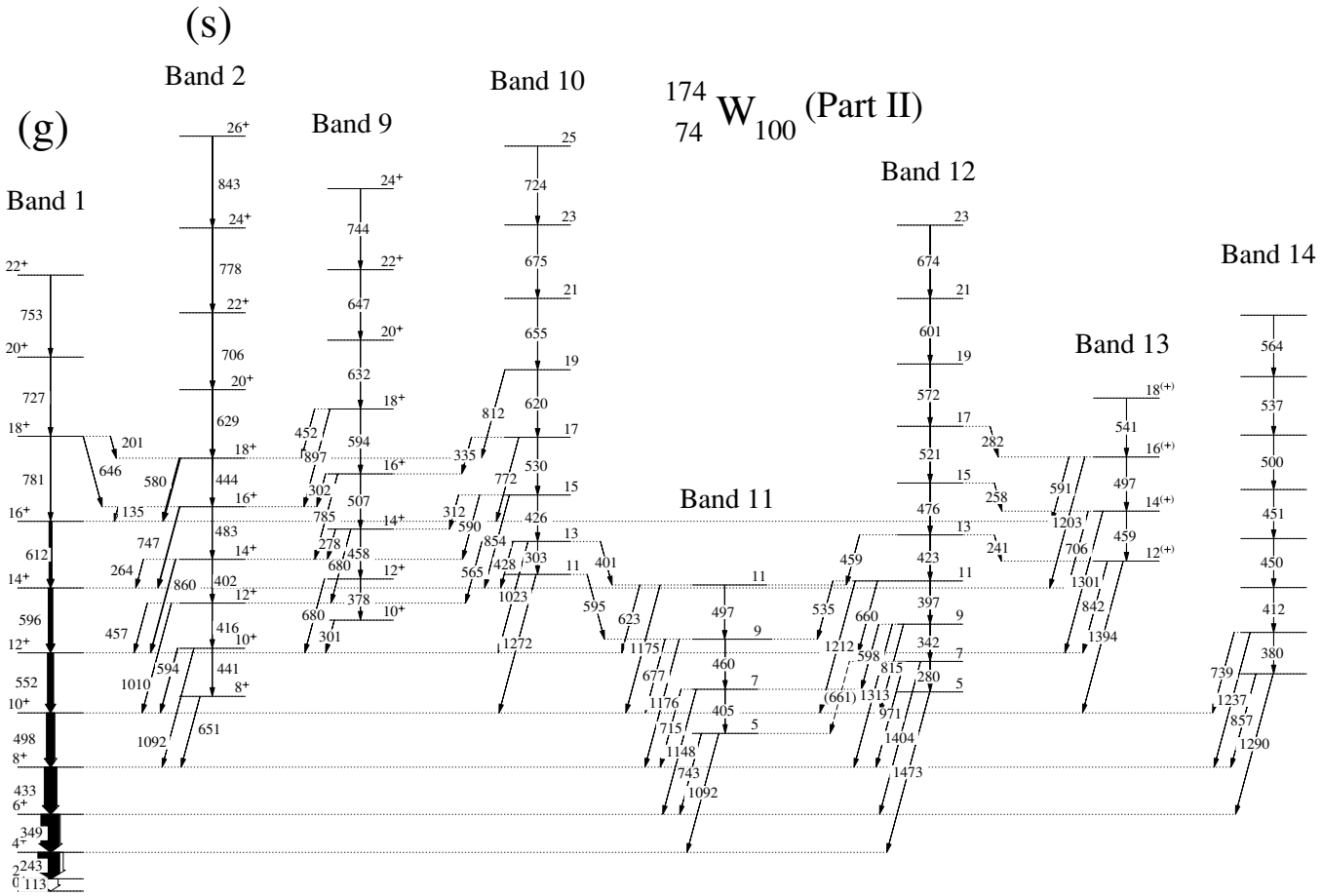

FIG. 2. Level scheme for ^{174}W displaying the positive parity and other sidebands.

but the placement and decay pattern of the isomeric bandhead state has been considerably modified. The previously reported 249-, 1314-, and 1349-keV γ rays have been observed from the decay of this isomer in addition to the 214-, 965-, and 1000-keV transitions; but there is no evidence for the 290- and 676-keV lines from the earlier study. The 214-keV transition deexcites the 6^- state in band 7 and not the 8^- isomeric state, as reported earlier. The decay out from the 8^- isomer proceeds through the 247-keV transition to the 7^- level in band 8. A half-life of 187 ns for the 8^- isomeric state had been reported earlier [7]. We have determined the half-life to be 158(3) ns based on the observed time difference between the transitions feeding and deexciting the 8^- isomer (Fig. 8). The spin assignment is based on the observed dipole character of the 247-keV transition. The tentative negative parity and $K^\pi = 8^-$ assignment follows from considerations of quasiparticle configurations discussed below.

G. Bands 17 and 18

The second isomeric state, at an excitation energy of 3516 keV, with a strongly coupled rotational band structure built on it, is new (Fig. 9). A half-life of 128(8) ns has been determined for this 3516-keV level (Fig. 10). The DCO ratios for the 1328- and 1879-keV decay transitions to the 10^+ and 12^+ states of band 1 are characteristic of either $I \rightarrow I$ or quadrupole transitions, suggesting a $I = K = 12$ assignment for the isomer. The positive parity assignment is based on the assumption of an $E2$ character for the 1879-keV transition. If this transition was of $M2$ character (which would imply negative parity for the $K = 12$ state), the 1328-keV γ ray would have to be of $E1$ character. An $M2/E1$ competition is unlikely, and the observed higher intensity for the 1879-keV transition, as compared to the 1328-keV line, would be difficult to understand in this scenario. With a 12^+ assignment, the $E2/M1$ competition follows the expected pattern. The decay of this isomer is in sharp contrast to that of the 8^- isomer: the 8^- state is seen to decay via a single transition from the isomeric bandhead to a member of band 8, which has a possible K value of 6, as discussed later. On the other hand, multiple decay branches are observed from the $K = 12$ isomer, the strongest of which are to band 1 (approximately 65%) through the 1328- and 1879-keV transitions. The transitions to bands 15 and 16 ($K = 8$) and band 19 ($K = 10$) constitute roughly 25% and 10% of the decay intensity, respectively.

H. Bands 19 and 20

Bands 19 and 20 form coupled rotational structures that are very weakly populated. The bandhead deexcites to band 1

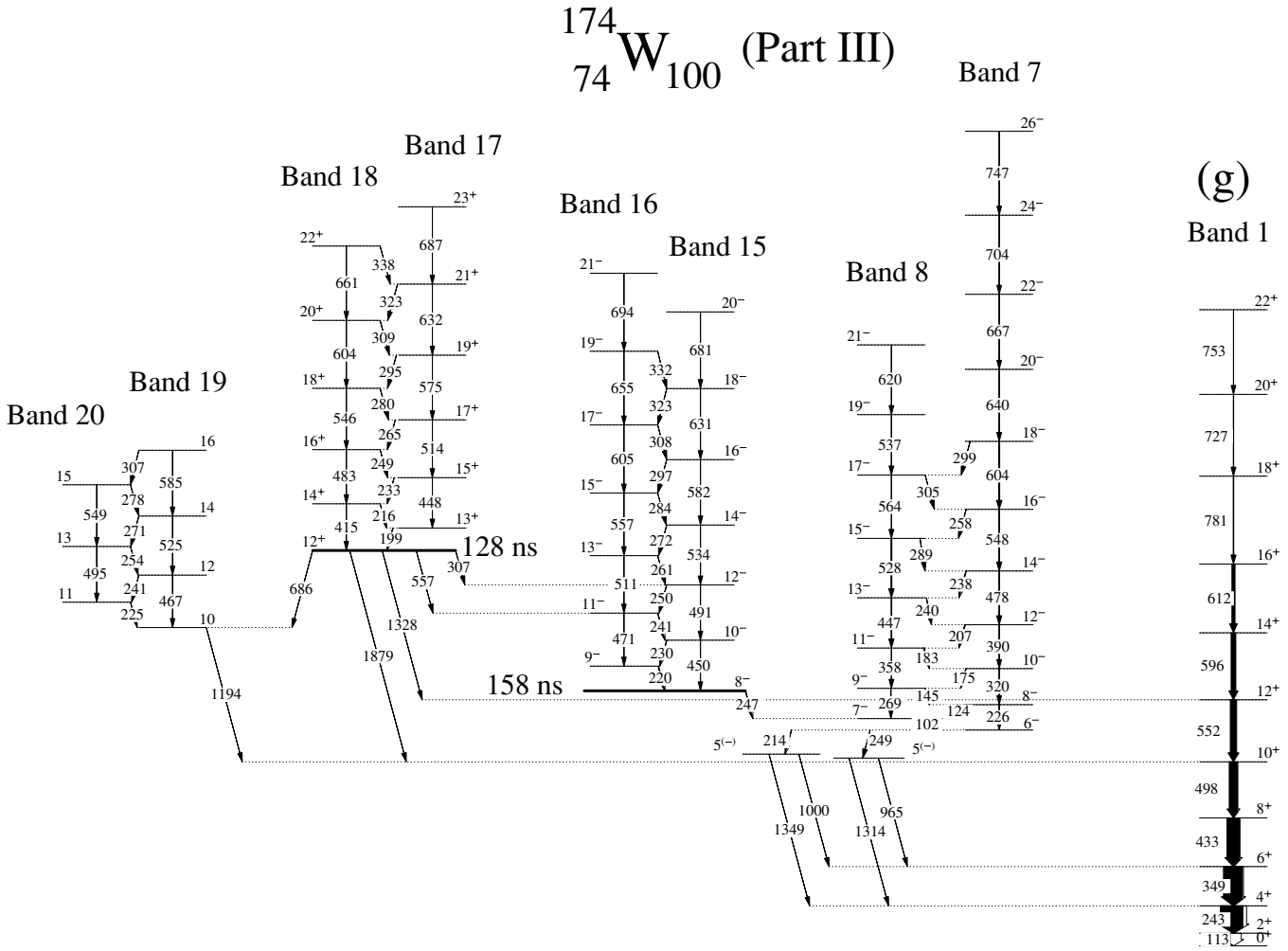

FIG. 3. Level scheme for ^{174}W with the high-K band structures.

through a 1194-keV γ ray. It was not possible to obtain accurate intensities for the rotational transitions in this band. A spin assignment of $10\hbar$ for the bandhead is based on the observed DCO ratio for the 1194-keV γ ray to the 10^+ state of band 1, which indicates that it is either a $I \rightarrow I$ or a quadrupole transition. The observation of a 686-keV transition from the

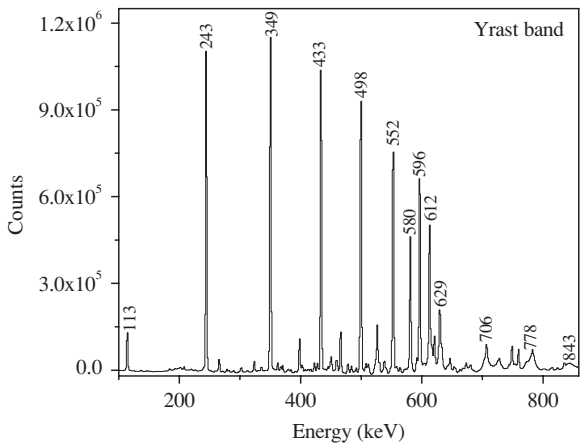

FIG. 4. Summed coincidence spectra for the transitions in the yrast sequence of ^{174}W.

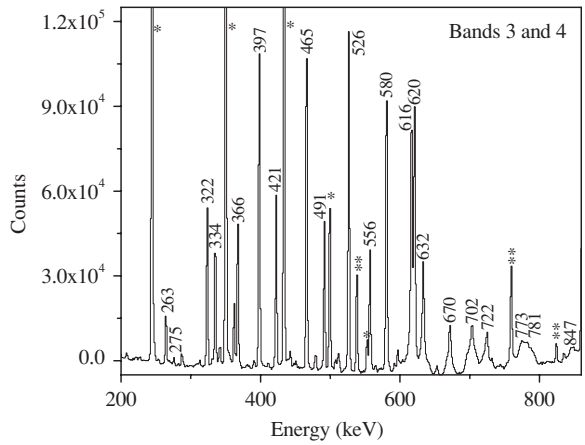

FIG. 5. Summed coincidence spectra showing in-band transitions in bands 3 and 4 of ^{174}W. γ rays labeled with single asterisks are part of the yrast sequence; double asterisks indicate out-of-band transitions from bands 3 and 4.

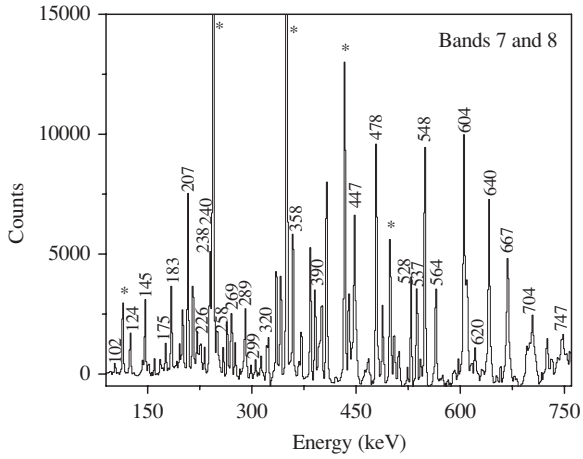

FIG. 6. Summed coincidence spectra representative of the transitions in bands 7 and 8; asterisks indicate coincident transitions in the yrast sequence.

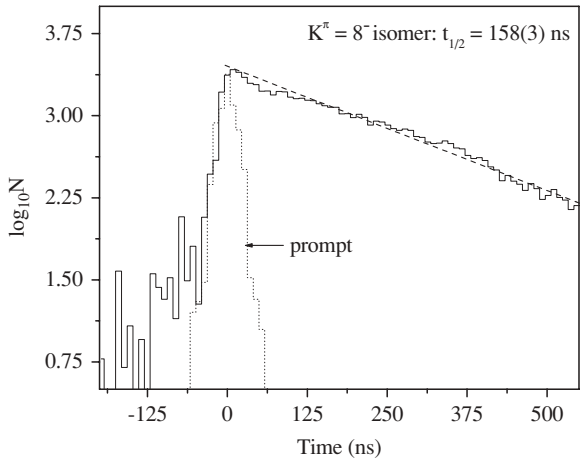

FIG. 8. Summed time difference spectrum obtained by gating on γ rays below and above the $K^{\pi} = 8^{-}$ isomer together with the exponential fit to the spectrum. The shape of a prompt time peak is also shown for comparison.

$K = 12$ isomer narrows the spin possibility to either 10 or 12. A spin of $12\hbar$ for the bandhead would bring these bands much closer to yrast compared to bands 17 and 18, and one would, therefore, expect these to have significantly higher intensity than what is observed. A $10\hbar$ assignment, therefore, appears to be more reasonable. A positive parity for this structure appears likely, based on the 686-keV transition observed from the $K^{\pi} = 12^{+}$ state, which has a higher probability of being an $E2$ rather than $M2$, based on the absence of a decay branch to the $I = 11$ member of band 20. Bands 19 and 20 will not be discussed further, due to the absence of adequate $M1/E2$ branching ratios and the uncertainty in the parity assignment.

IV. DISCUSSION

A. $K = 0$ and Intermediate K Bands

Calculations indicate that the nucleus ^{174}W exhibits an axially symmetric prolate shape over the range of observed rotational frequencies. Total Routhian surfaces (TRS) were calculated [16] for frequencies ranging from $\hbar\omega = 0.0$ to 0.5 MeV. The results are summarized in Fig. 11. It is evident that the prolate energy minimum persists for the indicated rotational frequencies. To determine the nucleonic configurations for the observed bands, a systematic comparison with neighboring nuclei has been done, and Woods-Saxon cranking calculations have been performed [16] to obtain the quasiparticle energy levels for ^{174}W. The bandhead states in the neighboring odd-A W isotopes [17,18] have spins $1/2^{-}$, $5/2^{-}$, and $7/2^{+}$, which is consistent with the [521]1/2, [512]5/2, and [633]7/2 quasineutron levels seen in the vicinity of the Fermi level in the quasiparticle diagrams (Fig. 12). The odd-A isotones, ^{173}Ta and ^{175}Re [19,20], are observed to have bands based upon the $5/2^{+}$, $7/2^{+}$, $5/2^{-}$ and $9/2^{-}$ states, which have been ascribed to the [402]5/2, [404]7/2,

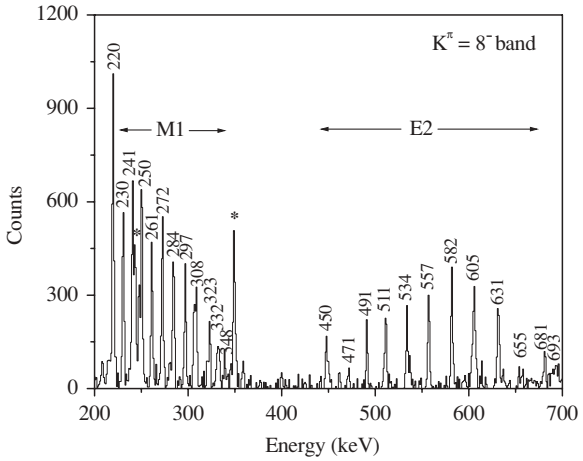

FIG. 7. Summed coincidence spectra with the transitions in the band built upon the $K^{\pi} = 8^{-}$ isomeric state; asterisks indicate transitions from band 1.

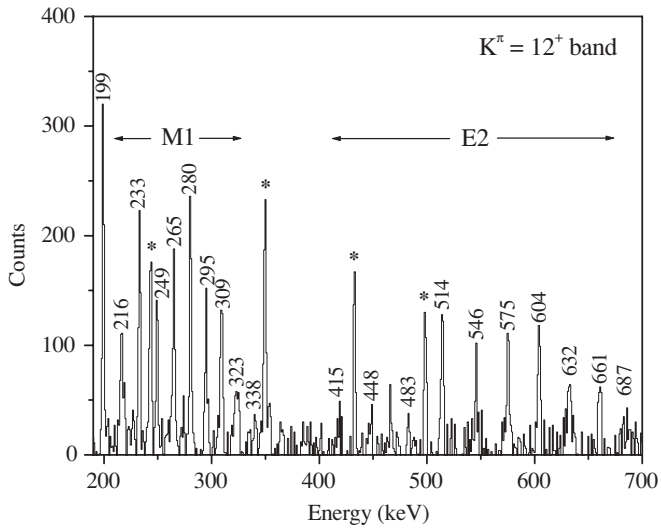

FIG. 9. Summed coincidence spectra showing the transitions in the $K^{\pi} = 12^{+}$ isomer band. Asterisks indicate transitions from band 1.

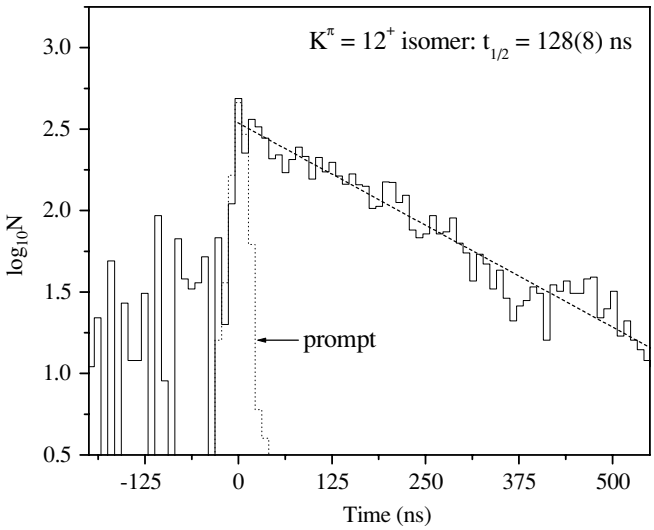

FIG. 10. Summed time difference spectrum obtained by gating on γ rays below and above the $K^\pi = 12^+$ isomer and the exponential fit to the spectrum. As in Fig. 8, a prompt peak is displayed for comparison.

[541]1/2, and [514]9/2 orbitals, respectively. These are the quasiproton orbitals observed in the vicinity of the Fermi level in the calculations (Fig. 13). The quasiparticle levels have been calculated using the deformation parameters $\beta_2 = 0.271$, $\beta_4 = -0.007$, and $\gamma = 0^\circ$, obtained from the potential energy surface calculations. The values for the proton and neutron pair gap energies have been taken from experimental odd-even mass differences following the prescription given in [21]. To differentiate between the various possible configurations for a given high-K band, g factors obtained from $M1/E2$ branching ratios were compared with those expected for the various possibilities (Table II). The experimental alignments are shown in Fig. 14, with Harris parameters of $J_0 = 26\hbar^2$/MeV and $J_1 = 67\hbar^4$/MeV^3 for the reference band [22].

1. K = 0 band: Bands 1 and 2

The yrast band undergoes a backbend at $\hbar\omega = 0.29$ MeV (Fig. 14). An inspection of the quasiparticle levels (Fig. 12) reveals that the first neutron $i_{13/2}$ (AB) crossing, because of the alignment of a pair of neutrons occupying the [633]7/2 orbital, is predicted to occur at a rotational frequency of $\hbar\omega = 0.28$ MeV. The predicted value is in excellent agreement with the observed frequency. The observation of a number of states in the g band (band 1) above and the s band (band 2) below the crossing region is rather uncommon. This would usually indicate a large interaction between the two bands. An experimental upper limit of $V_{gs} \leqslant 67$ keV for the mixing matrix element between the two bands can be immediately extracted, since the separation of the two closest levels with the same spin and parity in the two bands cannot be less than twice the mixing matrix element. In this case, since multiple decay branches between the two bands are observed over an extended spin range, a more detailed two-band mixing calculation, based on the measured in-band and out-of-band $E2$ transition strengths in the vicinity of the band crossing, can been performed to determine the mixing matrix element. The results of these calculations are summarized in Table III. A value of $V_{gs} \approx$ 65 keV reproduces the observed branching ratios quite well. This value differs from the value of ≈20 keV proposed in earlier work [7], where the analysis was based on excitation energies of yrast states only. The corresponding value obtained from the calculated quasiparticle levels (Fig. 12) is ≈80 keV.

The value of V_{gs} in ^{174}W ($N = 100$) is larger than that quoted in ^{176}W ($N = 102$) [5]. A reanalysis of the branching ratios

TABLE III. Branching ratios and interaction strengths V_{gs} for the g-s band crossing, using a two-band mixing model. $\frac{T^\gamma_{\rm out}}{T^\gamma_{\rm in}}$ denotes the ratio of out-of-band to in-band intensities observed from experiment, while $B(E2)$ is the reduced transition strength.

Nucleus	K^π_i	$\frac{T^\gamma_{\rm out}}{T^\gamma_{\rm in}}$	$\frac{B(E2)_{\rm out}}{B(E2)_{\rm in}}$ (expt.)	$\frac{B(E2)_{\rm out}}{B(E2)_{\rm in}}$ (calc.)	$\lvert V_{gs}\rvert$
^{174}W	18^+_g	0.53(5)	1.36(13)	2.54	64.9
	18^+_s	9.46(86)	2.54(23)	2.54	64.9
	16^+_s	4.31(48)	0.49(6)	0.18	64.9
	14^+_s	2.61(24)	0.058(5)	0.014	64.9
	12^+_s	1.10(11)	0.013(1)	0.001	64.9
^{176}W	18^+_g	0.59(10)	0.97(16)	1.20	29.9
	18^+_s	2.22(70)	1.20(37)	1.20	29.9
	16^+_s	1.83(44)	0.24(6)	0.22	29.9
	14^+_s	0.29(4)	0.009(1)	0.004	29.9

TABLE II. Proposed configuration assignments for bands in ^{174}W.

K^π	Configuration	$\frac{g_K - g_R}{Q_0}$(expected)	$\lvert\frac{g_K - g_R}{Q_0}\rvert$(experiment)	Observed band
4^-	ν^2 [633]7/2$^+$ ⊗ [521]1/2$^-$	−0.04	0.03(1)	Bands 3 and 4
4^-	π^2 [541]1/2$^-$ ⊗ [404]7/2$^+$	0.02	0.02(1)	
6^-_a	ν^2 [633]7/2$^+$ ⊗ [512]5/2$^-$	−0.09	0.02(1)	(Bands 5 and 6)
6^-_b	ν^2 [633]7/2$^+$ ⊗ [523]5/2$^-$	−0.04	0.04(1)	Bands 7 and 8
6^+	π^2 [404]7/2$^+$ ⊗ [402]5/2$^+$	0.10		
6^+	ν^2 [633]7/2$^+$ ⊗ [642]5/2$^+$	−0.09		
7^-	π^2 [514]9/2$^-$ ⊗ [402]5/2$^+$	0.15		
8^-	π^2 [514]9/2$^-$ ⊗ [404]7/2$^+$	0.10	0.06(1)	Bands 15 and 16
12^+	$\nu^2(4^-) \otimes \pi^2(8^-)$	0.05	0.04(1)	Bands 17 and 18
12^+	$\nu^2(6^+) \otimes \pi^2(6^+)$	0.004		

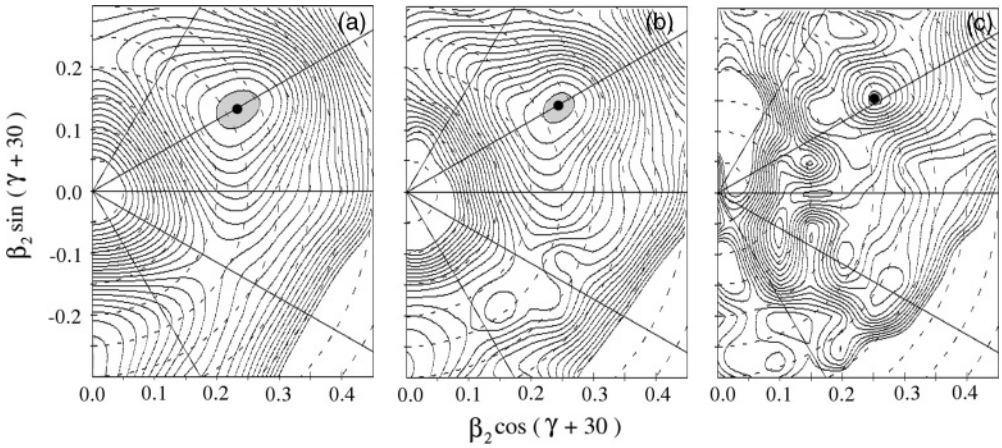

FIG. 11. Total Routhian surfaces for ^{174}W at (a) $\hbar\omega = 0.0$ MeV, (b) $\hbar\omega = 0.25$ MeV, and (c) $\hbar\omega = 0.50$ MeV. It is evident that an axially symmetric prolate shape (indicated by the shaded region and a black dot) is the lowest energy minimum up to high rotational frequencies.

from a two-band mixing calculation in ^{176}W yields a value of $V_{gs} \approx 30$ keV. The calculations are in much better agreement with measured values than those presented in Ref. [5]. The new comparison is summarized in Table III. The lower value of V_{gs} in ^{176}W is consistent with predictions as well as with observed systematics of a weaker interaction for $N = 102$ isotones in this region [23]. The band interaction scenario in ^{172}W is more complex [7] and has been discussed in terms of three-band mixing calculations [24]. Thus a direct comparison of mixing matrix elements between these isotopes does not offer any simple insight.

The exercise of comparing interaction strengths among the neighboring even-even isotones ^{172}Hf and ^{176}Os also does not provide any clear trends, particularly because no parallel states in g- and s-bands are observed in either nucleus, precluding any branching ratio measurements. A value of $V_{gs} \approx 20$ keV is quoted for ^{172}Hf based on two-band mixing calculations fitted to excitation energies of the yrast band members only [25]. In ^{176}Os, a similar exercise was used to quote rough limits of 40–60 keV for V_{gs} [26]. Subsequent analysis of the same data in ^{176}Os, using *three*-band mixing calculations incorporating a third deformed intruder band, yields values of V_{gs} that vary from 29 [27] to 174 keV [28].

Band 2, which appears to be mostly of s-band character above the 12^+ state, may interact with band 9 below this spin, as suggested by a downturn in the plot of $E_I - E_R$ versus I below a spin of $12\hbar$ (Fig. 15).

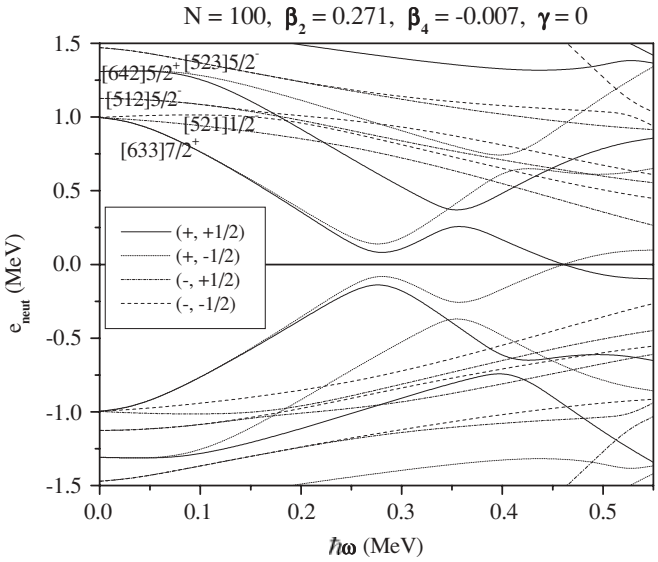

FIG. 12. Calculated neutron quasiparticle levels in ^{174}W as a function of rotational frequency. The AB crossing is evident at $\hbar\omega = 0.28$ MeV.

2. $K^\pi = 4^-$ band: Bands 3 and 4

The negative parity bands 3 and 4 appear to be signature partners, with large splitting, based on their observed structure. The lowest energy state at 1364 keV has the quantum numbers

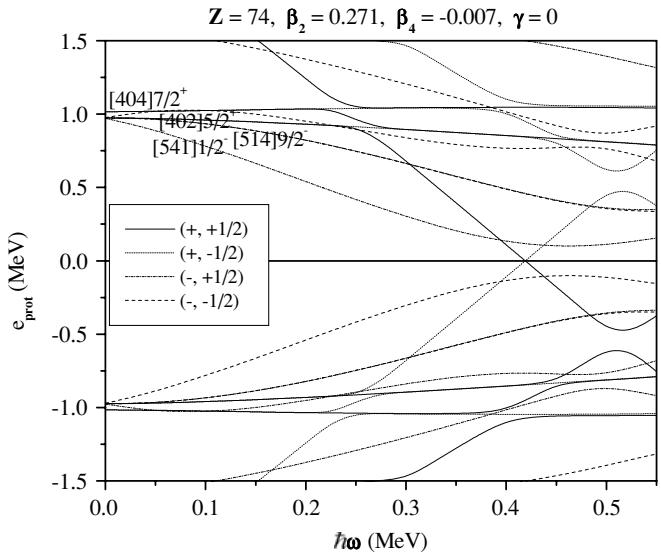

FIG. 13. Calculated proton quasiparticle levels in ^{174}W as a function of the rotational frequency.

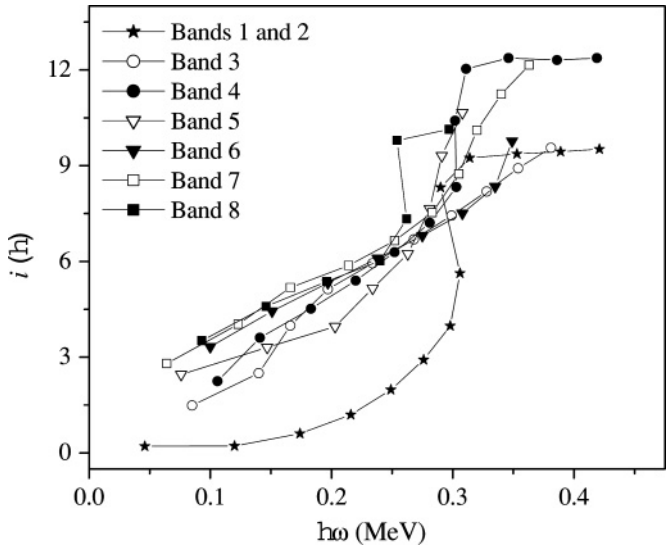

FIG. 14. Aligned angular momentum as a function of rotational frequency for selected bands in ^{174}W. The yrast states from bands 1 and 2 (g and s band) have been shown together to illustrate the alignment gain from the first neutron crossing.

$I^\pi = 4^-$. Bands built upon a 4^- state have been observed in the neighboring even W isotopes, ^{172}W [29] and ^{176}W [5]. The excitation energies of these 4^- levels in the ^{172,174,176}W isotopes are in close proximity being 1434, 1364, and 1302 keV, respectively. In ^{172}W, only a few transitions are observed in the band and an octupole vibrational structure is suggested. In contrast, in both ^{174}W and ^{176}W, this band (with $I^\pi = 4^-$ and $I^\pi = 5^-$ as the lowest energy states of the signature partners) is traced up to high spins ($>20\hbar$). In both these isotopes, the structure of the band at higher spins resembles that of a 2-qp band. Both possibilities, viz., octupole and 2-qp structure, have been considered in the case of ^{176}W, and it has been argued [5] that a 2-qp structure is most probable. In ^{174}W as well, the 2-qp contribution to the structure appears to be dominant, although a component of vibrational character in the level wave functions cannot be ruled out. There are two possible configurations which can generate $I^\pi = 4^-$, viz., $\nu^2[633]7/2^+ \otimes [521]1/2^-$ and $\pi^2[541]1/2^- \otimes [404]7/2^+$. The $|(g_K - g_R)/Q_0|$ value for this band, extracted from the $M1/E2$ branching ratios, is 0.03(1), consistent with the expected values for both the two-quasineutron (-0.04) and two-quasiproton (0.02) configurations mentioned above. A two-quasineutron assignment appears more probable for the following reasons. The two-quasineutron configuration is expected to generate the lowest negative parity band structure, which experimentally corresponds to bands 3 and 4. Furthermore, the experimental $|(g_K - g_R)/Q_0|$ values near the bandhead state are somewhat closer to 0.04, but reduce with increasing spin, leading to an effective value of 0.03(1) for the band. The reduction could possibly be attributed to a mixing with bands 5 and 6, which most likely are associated with a two-quasiproton configuration, as will be discussed later. The above considerations are consistent with the $\nu^2[633]7/2^+ \otimes [521]1/2^-$ configuration for bands 3 and 4. With increasing spin, the two-quasiproton contribution appears to become more dominant, as evidenced by the decrease in $(g_K - g_R)/Q_0$ values, and the observed alignment in band 4 at $\hbar\omega \approx 0.3$ MeV, which is not possible for a pure two-quasineutron configuration. Band 4 probably acquires more of a two-quasiproton character, and band 6 becomes predominantly two quasineutron in nature around a spin of $17\hbar$. This would account for the observed neutron alignments in bands 4 and 5 at $\hbar\omega \approx 0.3$ MeV and the absence of those alignments at this frequency in bands 3 and 6.

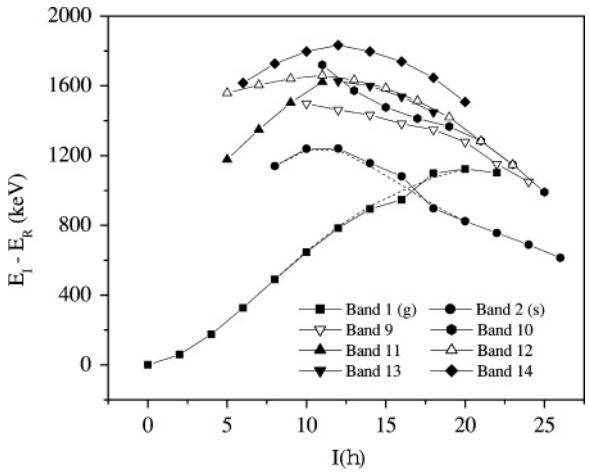

FIG. 15. Excitation energy E_I minus a rigid rotor reference E_R for the bands in Part II of the level scheme (Fig. 2). A rigid rotor reference of $E_R = 9^* I(I+1)$ keV has been subtracted from the level energies. The g- and s-band crossing is evident at $\approx 16\,\hbar$. The unperturbed trajectories of the g and s bands (from two-band mixing calculations) are indicated by dashed lines. The other sidebands are also shown for comparison.

3. Bands 5 and 6

There is considerable K mixing of bands 5 and 6 with bands 3 and 4 as well as with bands 7 and 8. The decays to the ground state band from bands 3 and 5 and those from bands 4 and 6 are very similar. However, in addition to these out-of-band decays, the lowest spin members of both bands 5 and 6 are also seen to have strong decays toward the 4^- and 5^- levels in bands 3 and 4. Two possible configuration scenarios exist. One configuration that yields $K^\pi = 6^-$ for the bandhead is $\nu^2[633]7/2^+ \otimes [512]5/2^-$ with an expected $(g_K - g_R)/Q_0$ value of -0.09. The other possibility is that the bandhead has not been reached at $I^\pi = 6^-$ in band 5. With $K^\pi = 4^-$ for the bandhead, a possible configuration is $\pi^2[541]1/2^- \otimes [404]7/2^+$, with an expected $(g_K - g_R)/Q_0$ value of 0.02. While the observed $(g_K - g_R)/Q_0$ value of 0.02(1) would seem to be fit better with the $\pi^2[541]1/2^- \otimes [404]7/2^+$ configuration, this value is based on the branching ratios extracted using only two weak $M1$ transitions observed linking bands 5 and 6. The 2-proton configuration would also make it difficult to understand why bands 5 and 6 mix strongly with bands 3 and 4 as well as bands 7 and 8, both of which have 2-neutron configurations. Thus, while neither configuration can be entirely ruled out by the present

measurements, the $\nu^2[633]7/2^+ \otimes [512]5/2^-$ configuration is perhaps more likely.

4. $K^\pi = 6^-$ band: Bands 7 and 8

Bands 7 and 8 appear to be strongly coupled signature partners based on the same intrinsic configuration. Based on the lowest 2-qp excitations able to generate $K^\pi = 6^-$, two possibilities emerge for this band, viz., $\nu^2[633]7/2^+ \otimes [523]5/2^-$ and $\nu^2[633]7/2^+ \otimes [512]5/2^-$. To differentiate between these two, expected and measured $(g_K - g_R)/Q_0$ values were compared. The expected values for the two configurations above are -0.04 and -0.09, respectively. The value for the $\nu^2[633]7/2^+ \otimes [523]5/2^-$ configuration is in excellent agreement with the measured absolute value of 0.04(1). Therefore, bands 7 and 8 are most probably associated with this configuration.

5. Bands 9 to 13

The limited experimental information on bands 9 to 13 allow only a rudimentary discussion on their possible structures. A band somewhat similar in its decay properties to band 9 is observed in the neighboring even-even isotone ^{172}Hf, labeled band 5 in Ref. [30]. In both cases, out-of-band transitions to the yrast band are observed over an extended region of spin. A vibrational character was conjectured for the ^{172}Hf band, based on the multiple linking transitions and similar alignments to the yrast band above the first crossing. While the excitation energy of band 9 in ^{174}W approximately follows the trajectory of the *s* band both above and below the first crossing, it is interesting to note that the out-of-band decays from its lower states proceed to band 1 before the crossing while the decays from higher spin states after the crossing are to the *s* band (band 2). The structure of band 10 is similar to that of band 9 in this respect. At higher spins, band 10 could be interpreted as the signature partner of band 9 (with large splitting) on the basis of the observed energetics and the presence of two linking transitions between the two bands. However, in the absence of a reasonably firm parity assignment for band 10, this sequence is not discussed further. Band 11 is probably of vibrational character, as evidenced from the plot of excitation energies (minus a rigid rotor reference) for bands 1 and 11 (Fig. 15). Band 13 could be interpreted as the signature partner to band 12, based on the links between the two structures and the energetics. However, that interpretation does not explain the observation of band 12 down to a spin of $5\hbar$, while band 13 is seen only above $12\hbar$.

B. High-*K* isomeric structures

1. $K^\pi = 8^-$ band

Two high-*K* isomers have been observed in the level structure of ^{174}W. The first is a 2-qp, $K^\pi = 8^-$ isomer with a half-life of 158(3) ns, on which bands 15 and 16 are built; the second is a 4-qp, $K^\pi = 12^+$ isomer, with $t_{1/2} = 128(8)$ ns, on which bands 17 and 18 are based. Bands 15 and 16 are two strongly coupled signature partners, with almost no signature splitting. The only 2-qp configuration from proton or neutron orbitals in the vicinity of the Fermi level which yields eight units of angular momentum is $\pi^2[514]9/2^- \otimes [404]7/2^+$. The expected $(g_K - g_R)/Q_0$ value for the configuration is 0.10, in reasonable agreement with the experimental value of 0.06(1). This appears to bear out the assignment of the above-mentioned two-quasiproton configuration for bands 15 and 16.

The only observed decay of the 8^- isomer occurs toward the 7^- level in band 8, with $K = 6$. This is an $M1$ transition with $\Delta K = 2$. The reduced hindrance factor f_ν is defined as $f_\nu = F^{1/\nu} = [\frac{T^\gamma_{1/2}}{T^W_{1/2}}]^{1/\nu}$, where $T^\gamma_{1/2}$ is the partial γ-ray half-life, $T^W_{1/2}$ is the corresponding Weisskopf estimate, and $\nu = \Delta K - \lambda$ is the degree of *K* forbiddenness of the transition. In this case, since $\nu = 1$, the reduced hindrance f_ν is the same as the hindrance factor *F*. The large hindrance of the decay ($f_\nu = F = 1.4 \times 10^5$) from the $K^\pi = 8^-$ state to band 8 through the 247-keV transition is typical [1,31] of *K* isomers. The $K^\pi = 12^+$ isomer, however, has a more interesting decay pattern, as discussed below.

2. $K^\pi = 12^+$ band

The major decay branches from the $K = 12$ isomer are to band 1. For *K*-forbidden decays with large ΔK and low reduced hindrance values reported earlier in this mass region, a fragmented decay pattern with a large number of decay branches to final states with a broad range of *K* values is more typical. For example, the $K^\pi = 14^+$ 4-qp isomer in ^{174}Hf decays via approximately 20 direct branches to 16 different band structures with *K* values ranging from 0 to 12 [32], while more than ten branches are observed for the decay of a $K^\pi = 33/2^+$ 5-qp isomer in ^{181}Os. In contrast, only five direct transitions are observed out of the 12^+ isomeric state in ^{174}W, with two $\Delta K = 12$ branches to the *g* band carrying the major fraction of the intensity. Since the $K = 12$ isomer also decays to the 8^- isomer, it is reasonable to assume that the configuration of the 12^+ state includes a $\pi^2[514]9/2^- \otimes [404]7/2^+$ component. In order to obtain $K^\pi = 12^+$, this configuration needs to be coupled to a 4^-, 2-qp structure. The lowest such structure has the configuration $\nu^2[633]7/2^+ \otimes [521]1/2^-$. The contribution of the $\nu[633]7/2^+$ orbital would also account for the high degree of alignment in the band (Fig. 14). The $K^\pi = 4^-$, two-quasiproton configuration (Table II) is excluded by the Pauli principle. The experimental $(g_K - g_R)/Q_0$ value for this band is 0.04(1), which is in good agreement with the expected value of 0.05 for the $\pi^2 8^- \otimes \nu^2 4^-$ configuration. The other possible $K^\pi = 12^+$ configuration would have led to a significantly different $(g_K - g_R)/Q_0$ value (Table II). Confirmation of the contributions to the 4-qp, $K^\pi = 12^+$ state from the $K^\pi = 4^-$ and 8^-, 2-qp structures is obtained from an inspection of the excitation energies of the relevant band-heads. The excitation energy of the $K^\pi = 12^+$ level is $E_x = 3516$ keV, while the sum of the $K^\pi = 4^-$ and 8^- energies is 3632 keV. The energy of the 4-qp state is slightly lower than

the sum of the 2-qp energies as would be expected as a result of residual interactions; the difference in the energies (116 keV) provides a measure of their magnitude. This value compares well with other 4-qp isomers in this region. For example, the $K^\pi = 12^+$ isomer in ^{172}Hf (108 keV) [33] and the $K^\pi = 14^+$ isomer in ^{174}Hf (200 keV) [32] exhibit residual interactions of the same magnitude. A comparison with the $K^\pi = 14^+$ isomer in ^{176}W [5] is not possible, since the band built upon the 2-qp, $K^\pi = 6^-$ configuration, which contributes to the 4-qp, $K^\pi = 14^+$ configuration, has not been observed in this instance.

3. Systematics of 4-qp isomers

Isomeric states with 4-qp character have been identified in many neighboring nuclei. Here, specific cases in nearest neighbors, viz., ^{172,174}Hf [32,33] and ^{176}W [5], are discussed to outline the similarity in underlying configurations and contrast the decay mechanisms. The $N = 100$ isotones ^{172}Hf and ^{174}W have 4-qp, $K^\pi = 12^+$ structures, while the $N = 102$ isotones ^{174}Hf and ^{176}W have 4-qp, $K^\pi = 14^+$ stuctures. All of these high-K states have $\nu^2\pi^2$ configurations with the same $[404]7/2^+$ and $[514]9/2^-$ proton orbitals. The $\nu[633]7/2^+$ orbital is also common to all those isomers. For the $N = 100$ isotones, the $\nu[521]1/2^-$ orbital provides the remainder of the contribution, while for $N = 102$, the $\nu[512]5/2^-$ orbital contributes. This can be easily understood in terms of the neutron Fermi level being higher for $N = 102$, bringing the $[512]5/2^-$ state closer to the Fermi level.

Remarkably, these particular 4-qp states in ^{172}Hf, ^{174,176}W have dominant decay branches to the respective g band or $K = 0$ states, which are the most K forbidden. The largest (and major) fraction of the decay to the g band is seen in ^{174}W. (In the case of ^{174}Hf, in contrast, the main decay branch is to the $K = 6$ band). In all of these cases, the decay intensity is fragmented over a number of paths. The reduced hindrances for the cases where the decays occur primarily to the $K = 0$ states are of the order $f_\nu \approx 3$–4. While the extracted f_ν of 3.8 for the 1879-keV $E2$ decay of the 12^+ state is compatible with such systematics, the hindrance factor stands out as an exception in model calculations that have been otherwise reasonably successful in explaining the systematics of such anomalously fast transitions with large ΔK in this mass region, as discussed below.

4. Decay mechanisms of multi-qp K isomers

A primary motivation for the present work was to investigate anomalously fast K-forbidden decays of multi-qp isomers in the Hf-W-Os region in a systematic manner. The new 4-qp isomer in ^{174}W, which exhibits multiple K-forbidden decay branches, provides an ideal candidate for such a test, given the similarity in its underlying configuration with previously observed 4-qp isomers in its immediate neighbors. As mentioned previously, one of the early mechanisms proposed to explain the unusually reduced hindrances for these K-forbidden decays was a tunneling of the nucleus through a barrier in the γ degree of freedom [2] along a line of constant β deformation. The key parameter in this model that lends itself to a systematic examination is the energy barrier along the γ-deformation axis through which the axially deformed nucleus is hypothesized to tunnel from the high-K bandhead (where intrinsic nucleonic spins are aligned along the symmetry axis) to low-K states (where the angular momentum of collective rotation is aligned perpendicular to the symmetry axis).

Decreasing excitation energies of 2^+ γ-vibrational bandheads with increasing Z in this region imply a softening of the potential in the γ degree of freedom, which translates to a lowering of γ-tunneling barriers as one progresses from Hf ($Z = 72$) to Os ($Z = 76$) nuclei. More refined and systematic γ-tunneling calculations [6] have been performed for a large number of isomer decays in this mass region. In this model, the Nilsson-Strutinsky method is used with dynamic pairing correlations included within the random-phase approximation to calculate the least *action* path in the β-γ shape landscape. The action W is related to the tunneling probability T via the simple expression $T \propto \exp -2W/\hbar$ (see Ref. [6] for details). These calculations have been very successful in describing a large body of isomer decays in this region. The hindrance factors calculated in this model either equal or exceed the experimentally measured values. In cases where this model overestimates the hindrance, it is reasonable to conjecture that decay mechanisms other than γ tunneling may contribute to faster transition rates and lower experimentally measured hindrance factors. There were *no* examples [6] where γ-tunneling calculations grossly *under predicted* measured hindrances.

Similar calculations were performed for the new $K = 12$ isomer decay in ^{174}W. The calculated action for $I = 12$ states in Hf, W, and Os isotopes are shown in Fig. 16, as a function of neutron number, where ^{174}W ($N = 100$) is seen to follow the expected systematic trend. The unexpected result is the large discrepancy, *opposite* to all previous examples, between the measured and calculated hindrance factors. The measured hindrance factor F_{exp} for the 1879-keV $E2$ transition from the $K = 12$ isomeric bandhead to the 10^+ state of ground state band is 7.3×10^5, three orders of magnitude *higher* than the

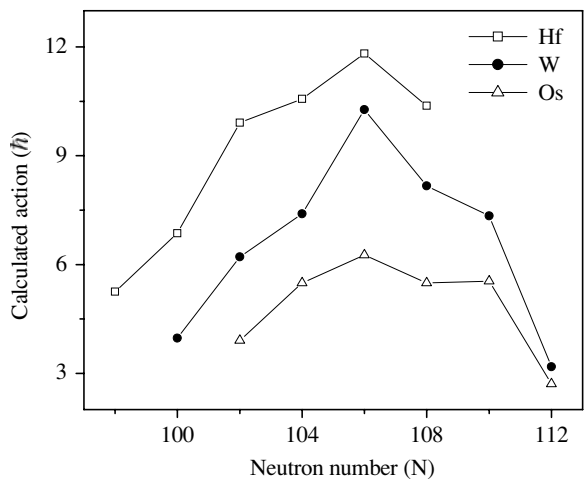

FIG. 16. Calculated action (in units of $\hbar$) for $I = 12$ states in the Hf, W, and Os isotopes.

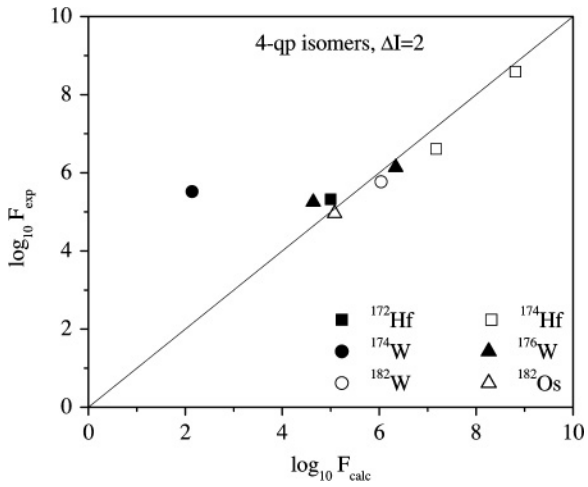

FIG. 17. Measured vs calculated hindrance F for few selected 4-qp isomers in the $A \approx 180$ region. The predictions of the γ-tunneling calculations are in agreement with experiment, except for the case of the $K = 12$ isomer in ^{174}W.

calculated value F_{calc} of 2.6×10^2. For the same bandhead configuration in ^{172}Hf, $F_{\text{calc}} = 1.0 \times 10^5$, which compares well with $F_{\text{exp}} = 2.1 \times 10^5$, using a 1-ns measured upper limit for the state half-life [30]. To highlight the discrepancy, measured versus calculated hindrance factors from $\Delta I = 2$ decays from a selected subset of 4-qp isomers are shown in Fig. 17. In the figure, points that fall along the diagonal are those where γ tunneling could be said to suffice as the primary mechanism for the decay. For points below the diagonal, other decay mechanisms could contribute toward a lower measured hindrance. On the contrary, points far above the diagonal, where the experimental hindrances are much larger than γ-tunneling predictions, are not at all understandable within this logic. As seen in the figure, γ-tunneling calculations are in general agreement with most observed decays, the only striking exception being the $K^\pi = 12^+$ isomer in ^{174}W. Since there are no surprises evident in the calculated tunneling barrier, it is difficult to understand the *increase* by three orders of magnitude in the measured hindrance compared to predictions from this otherwise successful model.

In contrast to γ tunneling, which invokes shape fluctuations and the role of triaxial degrees of freedom in the isomer decay, more traditional Coriolis K-mixing mechanisms have been proposed to explain, for example, the decay of 4-qp isomers in ^{172,174}Hf [32,33]. In these, admixtures of high-K components in the final state are considered as the primary reason for reducing the expected decay hindrances. The $K^\pi = 14^+$ isomer in ^{174}Hf is observed to decay to, among other states, an $I^\pi = 12^+$ state. The special configuration proposed [32] for this 12^+ state in ^{174}Hf is a coupling of two $i_{13/2}$ neutrons to form a high-K (Fermi-aligned or t band) configuration, unlike the more usual $K = 0$ coupling in a traditional s band. In ^{172}Hf, for the decay of the $K^\pi = 12^+$ level, although no state which might be part of a t band was identified, the small decay hindrance was discussed [33] in terms of a mixing of higher-K components in the g band, with increasing spin. In ^{174}W, unlike the situation in ^{172,174}Hf, a band (Band 2) arising from the alignment of two $i_{13/2}$ neutrons, has been identified over a considerable range of spin (8–26$\hbar$) and interpreted as an s band ($K = 0$) structure. There are no states identified in ^{174}W with t-band characteristics. If the s band did indeed have contributions from higher-K components, the absence of direct decays from the $K = 12$ isomer to s-band members is difficult to reconcile, given the observation of a strong decay branch to the g band.

A third mechanism that has been discussed [34] for anomalously fast decays of multi-qp K isomers is statistical mixing of the isomer with available states having the same spin and parity but lower K values; the higher the level density, the greater the mixing. Reduced hindrance factors f_ν are observed to decrease with increasing excitation energy (and density of states) above the yrast line for multi-qp isomers. A rough estimate of this correlation is presented in Ref. [34], assuming that the density of states increases exponentially with $\sqrt{\Delta E}$, where $\Delta E = E_K - E_R$, the excitation energy of the isomer relative to a common rigid rotor reference for a few nuclei with $A \approx 180$ (see Ref. [34] for details). While the decay of the new $K = 12$ isomer in ^{174}W lies within the general scatter of experimental data points in such an f_ν versus ΔE plot, it is difficult to venture beyond a qualitative agreement in trends between experiment and estimate. Large deviations in specific cases, together with inadequate constraining and normalization parameters in the model, do not allow for a detailed quantitative analysis of hindrance factors. The decay of the $K = 12$ isomer in ^{174}W, therefore, would require consideration of mechanisms other than those suggested by this simple model.

V. CONCLUSION

The level structure of ^{174}W has been considerably expanded, with 16 new bands being placed in the level scheme and the extension of the previously known three bands to higher spins. Woods-Saxon cranking calculations have been performed to calculate the quasiparticle energy levels and total Routhian surfaces for ^{174}W. Configuration assignments have been proposed for most of the observed bands, based on the calculated quasiparticle levels and g factors obtained from $M1/E2$ branching ratios. Two of the new structures are built upon the $K^\pi = 8^-$ and 12^+ isomeric 2- and 4-qp states, with half-lives of 158(3) and 128(8) ns, respectively. The new $K^\pi = 12^+$ isomeric state is observed to decay predominantly to the $K = 0$ yrast band, with weaker branches to intermediate-K states. For the decay of this isomer to the yrast band, γ-tunneling calculations predict a hindrance which is three orders of magnitude smaller than what is actually observed. A satisfactory explanation of this difference remains to be found.

ACKNOWLEDGMENTS

This work was supported by the U.S. Department of Energy, Office of Nuclear Physics, under Grants DE-FG02-94ER40848 and W-31-109-ENG-38.

[1] K. E. G. Löbner, Phys. Lett. **B26**, 369 (1968).
[2] T. Bengtsson, R. A. Broglia, E. Vigezzi, F. Barranco, F. Dönau, and Jing-ye Zhang, Phys. Rev. Lett. **62**, 2448 (1989).
[3] P. Chowdhury, B. Fabricius, C. Christensen, F. Azgui, S. Bjørnholm, J. Borggreen, A. Holm, J. Pedersen, G. Sletten, M. A. Bentley, D. Howe, A. R. Mokhtar, J. D. Morrison, J. F. Sharpey-Schafer, P. M. Walker, and R. M. Lieder, Nucl. Phys. **A485**, 136 (1988).
[4] B. Crowell, P. Chowdhury, S. J. Freeman, C. J. Lister, M. P. Carpenter, R. G. Henry, R. V. F. Janssens, T. L. Khoo, T. Lauritsen, Y. Liang, F. Soramel, and I. G. Bearden, Phys. Rev. Lett. **72**, 1164 (1994).
[5] B. Crowell, P. Chowdhury, D. J. Blumenthal, S. J. Freeman, C. J. Lister, M. P. Carpenter, R. G. Henry, R. V. F. Janssens, T. L. Khoo, T. Lauritsen, Y. Liang, F. Soramel, and I. G. Bearden, Phys. Rev. C **53**, 1173 (1996).
[6] K. Narimatsu, Y. R. Shimizu, and T. Shizuma, Nucl. Phys. **A601**, 69 (1996).
[7] G. D. Dracoulis, P. M. Walker, and A. Johnston, J. Phys. G **4**, 713 (1978).
[8] E. Seabury, P. Chowdhury, I. Ahmad, M. Carpenter, S. Fischer, R. V. F. Janssens, T. L. Khoo, T. Lauritsen, C. J. Lister, and D. Seweryniak, Bull. Am. Phys. Soc. **43**, 1223 (1998).
[9] P. Chowdhury, E. Seabury, K. Shaw, S. Sui, I. Ahmad, M. Carpenter, S. Fischer, R. V. F. Janssens, T. L. Khoo, T. Lauritsen, C. J. Lister, and D. Seweryniak, Bull. Am. Phys. Soc. **42**, 1105 (1997).
[10] I. Y. Lee, Nucl. Phys. **A520**, 641c (1990).
[11] D. C. Radford, Nucl. Instrum. Methods Phys. Res. A **361**, 297 (1995).
[12] H.-Q. Jin, TSCAN and related programs-A package to perform tape scanning and to manipulate matrices, RUTGERS-ORNL-UTK (1992–97).
[13] K. S. Krane, R. M. Steffen, and R. M. Wheeler, Nucl. Data Tables **11**, 351 (1973).
[14] A. Kramer-Flecken, Nucl. Instrum. Methods Phys. Res. A **275**, 333 (1989).
[15] J. Gascon, P. Taras, P. van Esbroek, H. R. Andrews, D. C. Radford, D. Ward, and A. Christy, Nucl. Phys. **A472**, 558 (1987).
[16] W. Nazarewicz, J. Dudek, R. Bengtsson, T. Bengtsson, and I. Ragnarsson, Nucl. Phys. **A435**, 397 (1985).
[17] P. M. Walker, G. D. Dracoulis, A. Johnston, J. R. Leigh, M. G. Slocombe, and I. F. Wright, J. Phys. G **2**, L197 (1976).
[18] P. M. Walker, G. D. Dracoulis, A. Johnston, J. R. Leigh, M. G. Slocombe, and I. F. Wright, J. Phys. G **4**, 1655 (1978).
[19] H. Carlsson, R. A. Bark, L. P. Ekstrom, A. Nordlund, H. Ryde, G. B. Hagemann, S. J. Freeman, H. J. Jensen, T. Lonnroth, M. J. Piiparinen, H. Schnack-Petersen, F. Ingebretsen, and P. O. Tjom, Nucl. Phys. **A592**, 89 (1995).
[20] T. Kibedi, G. D. Dracoulis, B. Fabricius, A. P. Byrne, and A. E. Stuchbery, Nucl. Phys. **A539**, 137 (1992).
[21] P. Möller and J. R. Nix, Nucl. Phys. **A536**, 20 (1992).
[22] S. M. Harris, Phys. Rev. **138**, B509 (1965).
[23] R. Bengtsson, S. Frauendorf, and F. R. May, At. Data Nucl. Data Tables **35**, 15 (1986).
[24] F. K. McGowan, N. R. Johnson, I. Y. Lee, C. Baktash, J. W. McConnell, M. N. Rao, M. Oshima, J. C. Wells, A. Larabee, L. L. Reidinger, R. Bengtsson, and Z. Xing, Nucl. Phys. **A530**, 490 (1991).
[25] G. D. Dracoulis, P. M. Walker, and A. Johnston, J. Phys. G **3**, L249 (1977).
[26] G. D. Dracoulis, C. Fahlander, and M. P. Fewell, Nucl. Phys. **A383**, 119 (1982).
[27] R. A. Bark, J. Phys. G **17**, 1209 (1991).
[28] T. Kibedi, G. D. Dracoulis, A. P. Byrne, and P. M. Davidson, Nucl. Phys. **A67**, 183 (1994).
[29] J. Espino, J. D. Garrett, G. B. Hagemann, P. O. Tjom, C.-H. Yu, M. Bergström, L. Carlen, L. P. Ekström, J. Lyttkens-Linden, H. Ryde, R. Bengtsson, T. Bengtsson, R. Chapman, D. Clarke, F. Khazaie, J. C. Lisle, and J. N. Mo, Nucl. Phys. **A567**, 377 (1994).
[30] D. M. Cullen, C. Baktash, M. J. Fitch, I. Frosch, R. W. Gray, N. R. Johnson, I. Y. Lee, A. O. Macchiavelli, W. Reviol, X.-H. Wang, and C.-H. Yu, Phys. Rev. C **52**, 2415 (1995).
[31] A. Bohr and B. R. Mottelson, *Nuclear Structure* (Benjamin, Reading, MA, 1975), Vol. II.
[32] N. L. Gjørup, P. M. Walker, G. Sletten, M. A. Bentley, B. Fabricius, and J. F. Sharpey-Schafer, Nucl. Phys. **A582**, 369 (1995).
[33] D. M. Cullen, A. T. Reed, D. E. Appelbe, A. N. Wilson, E. S. Paul, R. M. Clark, P. Fallon, I. Y. Lee, A. O. Macchiavelli, and R. W. MacLeod, Nucl. Phys. **A638**, 662 (1998).
[34] P. M. Walker, D. M. Cullen, C. S. Purry, D. E. Appelbe, A. P. Byrne, G. D. Dracoulis, T. Kibedi, F. G. Kondev, I. Y. Lee, A. O. Macchiavelli, A. T. Reed, P. H. Regan, and F. Xu, Phys. Lett. **B408**, 42 (1997).